EUROPEAN LABORATORY FOR PARTICLE PHYSICS

CERN-PPE/97-046
29th April 1997

Search for Scalar Top and Scalar Bottom Quarks at $\sqrt{s} = 170 - 172$ GeV in e^+e^- Collisions

The OPAL Collaboration

Abstract

A search for a scalar top quark has been performed using a total data sample of 10.4 pb^{-1} at centre-of-mass energies of $\sqrt{s}$ =170 and 172 GeV collected with the OPAL detector at LEP. No candidate events were observed. Combining this result with those obtained at $\sqrt{s} = 130$, 136 and 161 GeV, the 95% C.L. lower limit on the scalar top quark mass is 66.8 GeV, if the mixing angle between the supersymmetric partners of the left- and right-handed states of the top quark is smaller than $\frac{\pi}{4}$. If the mixing angle is zero, the limit is 73.3 GeV. These limits were obtained assuming that the scalar top quark decays into a charm quark and the lightest neutralino, and that the mass difference between the scalar top quark and the lightest neutralino is larger than 10 GeV. The complementary decay mode of the scalar top quark in which it decays into a bottom quark, a charged lepton and a scalar neutrino was also studied. From a similar analysis, a mass limit on the light scalar bottom quark was set at 69.7 GeV, for a mixing angle between the supersymmetric partners of the left- and right-handed states of the bottom quark of zero, and the mass difference between the scalar bottom quark and the lightest neutralino larger than 8 GeV.

(To be submitted to Zeit. Phys. C)

The OPAL Collaboration

K. Ackerstaff[8], G. Alexander[23], J. Allison[16], N. Altekamp[5], K.J. Anderson[9], S. Anderson[12], S. Arcelli[2], S. Asai[24], D. Axen[29], G. Azuelos[18,a], A.H. Ball[17], E. Barberio[8], R.J. Barlow[16], R. Bartoldus[3], J.R. Batley[5], S. Baumann[3], J. Bechtluft[14], C. Beeston[16], T. Behnke[8], A.N. Bell[1], K.W. Bell[20], G. Bella[23], S. Bentvelsen[8], P. Berlich[10], S. Bethke[14], O. Biebel[14], A. Biguzzi[5], S.D. Bird[16], V. Blobel[27], I.J. Bloodworth[1], J.E. Bloomer[1], M. Bobinski[10], P. Bock[11], D. Bonacorsi[2], M. Boutemeur[34], B.T. Bouwens[12], S. Braibant[12], L. Brigliadori[2], R.M. Brown[20], H.J. Burckhart[8], C. Burgard[8], R. Bürgin[10], P. Capiluppi[2], R.K. Carnegie[6], A.A. Carter[13], J.R. Carter[5], C.Y. Chang[17], D.G. Charlton[1,b], D. Chrisman[4], P.E.L. Clarke[15], I. Cohen[23], J.E. Conboy[15], O.C. Cooke[16], M. Cuffiani[2], S. Dado[22], C. Dallapiccola[17], G.M. Dallavalle[2], S. De Jong[12], L.A. del Pozo[4], K. Desch[3], M.S. Dixit[7], E. do Couto e Silva[12], M. Doucet[18], E. Duchovni[26], G. Duckeck[34], I.P. Duerdoth[16], D. Eatough[16], J.E.G. Edwards[16], P.G. Estabrooks[6], H.G. Evans[9], M. Evans[13], F. Fabbri[2], M. Fanti[2], A.A. Faust[30], F. Fiedler[27], M. Fierro[2], H.M. Fischer[3], I. Fleck[8], R. Folman[26], D.G. Fong[17], M. Foucher[17], A. Fürtjes[8], D.I. Futyan[16], P. Gagnon[7], J.W. Gary[4], J. Gascon[18], S.M. Gascon-Shotkin[17], N.I. Geddes[20], C. Geich-Gimbel[3], T. Geralis[20], G. Giacomelli[2], P. Giacomelli[4], R. Giacomelli[2], V. Gibson[5], W.R. Gibson[13], D.M. Gingrich[30,a], D. Glenzinski[9], J. Goldberg[22], M.J. Goodrick[5], W. Gorn[4], C. Grandi[2], E. Gross[26], J. Grunhaus[23], M. Gruwé[8], C. Hajdu[32], G.G. Hanson[12], M. Hansroul[8], M. Hapke[13], C.K. Hargrove[7], P.A. Hart[9], C. Hartmann[3], M. Hauschild[8], C.M. Hawkes[5], R. Hawkings[27], R.J. Hemingway[6], M. Herndon[17], G. Herten[10], R.D. Heuer[8], M.D. Hildreth[8], J.C. Hill[5], S.J. Hillier[1], T. Hilse[10], P.R. Hobson[25], R.J. Homer[1], A.K. Honma[28,a], D. Horváth[32,c], R. Howard[29], D.E. Hutchcroft[5], P. Igo-Kemenes[11], D.C. Imrie[25], M.R. Ingram[16], K. Ishii[24], A. Jawahery[17], P.W. Jeffreys[20], H. Jeremie[18], M. Jimack[1], A. Joly[18], C.R. Jones[5], G. Jones[16], M. Jones[6], U. Jost[11], P. Jovanovic[1], T.R. Junk[8], D. Karlen[6], V. Kartvelishvili[16], K. Kawagoe[24], T. Kawamoto[24], R.K. Keeler[28], R.G. Kellogg[17], B.W. Kennedy[20], J. Kirk[29], A. Klier[26], S. Kluth[8], T. Kobayashi[24], M. Kobel[10], D.S. Koetke[6], T.P. Kokott[3], M. Kolrep[10], S. Komamiya[24], T. Kress[11], P. Krieger[6], J. von Krogh[11], P. Kyberd[13], G.D. Lafferty[16], R. Lahmann[17], W.P. Lai[19], D. Lanske[14], J. Lauber[15], S.R. Lautenschlager[31], J.G. Layter[4], D. Lazic[22], A.M. Lee[31], E. Lefebvre[18], D. Lellouch[26], J. Letts[12], L. Levinson[26], S.L. Lloyd[13], F.K. Loebinger[16], G.D. Long[28], M.J. Losty[7], J. Ludwig[10], A. Macchiolo[2], A. Macpherson[30], M. Mannelli[8], S. Marcellini[2], C. Markus[3], A.J. Martin[13], J.P. Martin[18], G. Martinez[17], T. Mashimo[24], P. Mättig[3], W.J. McDonald[30], J. McKenna[29], E.A. Mckigney[15], T.J. McMahon[1], R.A. McPherson[8], F. Meijers[8], S. Menke[3], F.S. Merritt[9], H. Mes[7], J. Meyer[27], A. Michelini[2], G. Mikenberg[26], D.J. Miller[15], A. Mincer[22,e], R. Mir[26], W. Mohr[10], A. Montanari[2], T. Mori[24], M. Morii[24], U. Müller[3], K. Nagai[26], I. Nakamura[24], H.A. Neal[8], B. Nellen[3], R. Nisius[8], S.W. O'Neale[1], F.G. Oakham[7], F. Odorici[2], H.O. Ogren[12], N.J. Oldershaw[16], M.J. Oreglia[9], S. Orito[24], J. Pálinkás[33,d], G. Pásztor[32], J.R. Pater[16], G.N. Patrick[20], J. Patt[10], M.J. Pearce[1], S. Petzold[27], P. Pfeifenschneider[14], J.E. Pilcher[9], J. Pinfold[30], D.E. Plane[8], P. Poffenberger[28], B. Poli[2], A. Posthaus[3], H. Przysiezniak[30], D.L. Rees[1], D. Rigby[1], S. Robertson[28], S.A. Robins[22], N. Rodning[30], J.M. Roney[28], A. Rooke[15], E. Ros[8], A.M. Rossi[2], M. Rosvick[28], P. Routenburg[30], Y. Rozen[22], K. Runge[10], O. Runolfsson[8], U. Ruppel[14], D.R. Rust[12], R. Rylko[25], K. Sachs[10], T. Saeki[24], E.K.G. Sarkisyan[23], C. Sbarra[29], A.D. Schaile[34], O. Schaile[34], F. Scharf[3], P. Scharff-Hansen[8], P. Schenk[34], J. Schieck[11], P. Schleper[11], B. Schmitt[8], S. Schmitt[11], A. Schöning[8], M. Schröder[8], H.C. Schultz-Coulon[10], M. Schulz[8], M. Schumacher[3], C. Schwick[8], W.G. Scott[20], T.G. Shears[16], B.C. Shen[4], C.H. Shepherd-Themistocleous[8], P. Sherwood[15],

G.P. Siroli[2], A. Sittler[27], A. Skillman[15], A. Skuja[17], A.M. Smith[8], G.A. Snow[17], R. Sobie[28], S. Söldner-Rembold[10], R.W. Springer[30], M. Sproston[20], K. Stephens[16], J. Steuerer[27], B. Stockhausen[3], K. Stoll[10], D. Strom[19], P. Szymanski[20], R. Tafirout[18], S.D. Talbot[1], S. Tanaka[24], P. Taras[18], S. Tarem[22], R. Teuscher[8], M. Thiergen[10], M.A. Thomson[8], E. von Törne[3], S. Towers[6], I. Trigger[18], E. Tsur[23], A.S. Turcot[9], M.F. Turner-Watson[8], P. Utzat[11], R. Van Kooten[12], M. Verzocchi[10], P. Vikas[18], E.H. Vokurka[16], H. Voss[3], F. Wäckerle[10], A. Wagner[27], C.P. Ward[5], D.R. Ward[5], P.M. Watkins[1], A.T. Watson[1], N.K. Watson[1], P.S. Wells[8], N. Wermes[3], J.S. White[28], B. Wilkens[10], G.W. Wilson[27], J.A. Wilson[1], G. Wolf[26], T.R. Wyatt[16], S. Yamashita[24], G. Yekutieli[26], V. Zacek[18], D. Zer-Zion[8]

[1]School of Physics and Space Research, University of Birmingham, Birmingham B15 2TT, UK
[2]Dipartimento di Fisica dell' Università di Bologna and INFN, I-40126 Bologna, Italy
[3]Physikalisches Institut, Universität Bonn, D-53115 Bonn, Germany
[4]Department of Physics, University of California, Riverside CA 92521, USA
[5]Cavendish Laboratory, Cambridge CB3 0HE, UK
[6] Ottawa-Carleton Institute for Physics, Department of Physics, Carleton University, Ottawa, Ontario K1S 5B6, Canada
[7]Centre for Research in Particle Physics, Carleton University, Ottawa, Ontario K1S 5B6, Canada
[8]CERN, European Organisation for Particle Physics, CH-1211 Geneva 23, Switzerland
[9]Enrico Fermi Institute and Department of Physics, University of Chicago, Chicago IL 60637, USA
[10]Fakultät für Physik, Albert Ludwigs Universität, D-79104 Freiburg, Germany
[11]Physikalisches Institut, Universität Heidelberg, D-69120 Heidelberg, Germany
[12]Indiana University, Department of Physics, Swain Hall West 117, Bloomington IN 47405, USA
[13]Queen Mary and Westfield College, University of London, London E1 4NS, UK
[14]Technische Hochschule Aachen, III Physikalisches Institut, Sommerfeldstrasse 26-28, D-52056 Aachen, Germany
[15]University College London, London WC1E 6BT, UK
[16]Department of Physics, Schuster Laboratory, The University, Manchester M13 9PL, UK
[17]Department of Physics, University of Maryland, College Park, MD 20742, USA
[18]Laboratoire de Physique Nucléaire, Université de Montréal, Montréal, Quebec H3C 3J7, Canada
[19]University of Oregon, Department of Physics, Eugene OR 97403, USA
[20]Rutherford Appleton Laboratory, Chilton, Didcot, Oxfordshire OX11 0QX, UK
[22]Department of Physics, Technion-Israel Institute of Technology, Haifa 32000, Israel
[23]Department of Physics and Astronomy, Tel Aviv University, Tel Aviv 69978, Israel
[24]International Centre for Elementary Particle Physics and Department of Physics, University of Tokyo, Tokyo 113, and Kobe University, Kobe 657, Japan
[25]Brunel University, Uxbridge, Middlesex UB8 3PH, UK
[26]Particle Physics Department, Weizmann Institute of Science, Rehovot 76100, Israel
[27]Universität Hamburg/DESY, II Institut für Experimental Physik, Notkestrasse 85, D-22607 Hamburg, Germany
[28]University of Victoria, Department of Physics, P O Box 3055, Victoria BC V8W 3P6, Canada
[29]University of British Columbia, Department of Physics, Vancouver BC V6T 1Z1, Canada

[30]University of Alberta, Department of Physics, Edmonton AB T6G 2J1, Canada
[31]Duke University, Dept of Physics, Durham, NC 27708-0305, USA
[32]Research Institute for Particle and Nuclear Physics, H-1525 Budapest, P O Box 49, Hungary
[33]Institute of Nuclear Research, H-4001 Debrecen, P O Box 51, Hungary
[34]Ludwigs-Maximilians-Universität München, Sektion Physik, Am Coulombwall 1, D-85748 Garching, Germany

[a] and at TRIUMF, Vancouver, Canada V6T 2A3
[b] and Royal Society University Research Fellow
[c] and Institute of Nuclear Research, Debrecen, Hungary
[d] and Department of Experimental Physics, Lajos Kossuth University, Debrecen, Hungary
[e] and Depart of Physics, New York University, NY 1003, USA

1 Introduction

Supersymmetric (SUSY) extensions [1] of the Standard Model predict the existence of the bosonic partners of all known fermions. The scalar top quark ($\tilde{t}$), which is the bosonic partner of the top quark, can be the lightest charged supersymmetric particle for the following two reasons [2]: (1) The radiative correction to the $\tilde{t}$ mass through Higgsino-quark loops and Higgs-squark loops is negative. The correction is expected to be large for a heavy top quark mass as measured by the CDF and D0 Collaborations [3], since it is proportional to the square of the Yukawa coupling of the top quark. (2) Due to the mixing of supersymmetric partners of the right-handed and left-handed top quarks ($\tilde{t}_R$ and $\tilde{t}_L$) the resultant two mass eigenstates ($\tilde{t}_1$ and $\tilde{t}_2$) have a mass splitting. This mass splitting is expected to be very large for the large top quark mass. Hence the lighter mass eigenstate ($\tilde{t}_1$) can be lighter than any other charged SUSY particle, and also lighter than the top quark itself [2].

In addition, the scalar bottom quark ($\tilde{b}$) can be light, if $\tan\beta$, the ratio of vacuum expectation values of the two Higgs doublets, is as large as about 40. In this case, a large mixing of the right-handed and left-handed scalar bottom quarks ($\tilde{b}_R$ and $\tilde{b}_L$) occurs, and the resultant two mass eigenstates ($\tilde{b}_1$ and $\tilde{b}_2$) also have a large mass splitting [4]. The mass of the lighter mass eigenstate ($\tilde{b}_1$) may therefore be within the reach of LEP2.

Scalar top quark pairs and scalar bottom quark pairs are produced in e^+e^- annihilation via a virtual Z^0 boson or a virtual photon. In this paper it is assumed that either $\tilde{\chi}_1^0$ or $\tilde{\nu}$ is the only SUSY particle which is lighter than $\tilde{t}_1$ ($\tilde{b}_1$) and that R-parity is conserved. The dominant decay mode of the $\tilde{t}_1$ with the above assumptions is expected to be $\tilde{t}_1 \to c\tilde{\chi}_1^0$ or $\tilde{t}_1 \to b\tilde{\nu}\ell^+$, where $\tilde{\chi}_1^0$ is the lightest neutralino and $\tilde{\nu}$ is scalar neutrino. Both of these decay modes have been searched for. The dominant decay mode of the $\tilde{b}_1$ is expected to be $\tilde{b}_1 \to b\tilde{\chi}_1^0$. Under the assumption of R-parity conservation, the $\tilde{\chi}_1^0$ and $\tilde{\nu}$ are invisible in the detector. Thus, $\tilde{t}_1\bar{\tilde{t}}_1$ and $\tilde{b}_1\bar{\tilde{b}}_1$ events are characterised by two acoplanar jets [1] or two acoplanar jets plus two leptons, with missing energy.

The D0 Collaboration have reported a lower limit [5] on the $\tilde{t}_1$ mass of about 85 GeV (95 % C.L.) for the case that it decays into a charm quark and the lightest neutralino, $\tilde{\chi}_1^0$, and

[1]Two jets not back-to-back with each other in the plane perpendicular to the beam axis.

that the mass difference between $\tilde{t}_1$ and $\tilde{\chi}^0_1$ is larger than about 35 GeV. Searches at e^+e^- colliders are sensitive to a smaller mass difference and mass limits for the $\tilde{t}_1$ have been obtained around the Z^0 peak (LEP1) with the assumption that the $\tilde{t}_1$ decays into a charm quark and a $\tilde{\chi}^0_1$. A 95 % C.L. lower limit of about 45 GeV was obtained for a mass difference larger than 5 GeV [6]. Previous searches at centre-of-mass energies of $\sqrt{s}$= 130, 136 [7] and 161 GeV [8] have improved the limit on the mass of the $\tilde{t}_1$ to 58.7 GeV if the mixing angle between $\tilde{t}_R$ and $\tilde{t}_L$ is smaller than $\pi/4$ and if the mass difference between $\tilde{t}_1$ and $\tilde{\chi}^0_1$ is larger than 10 GeV.

In the autumn of 1996 the LEP e^+e^- collider at CERN was run for the first time at centre-of-mass energies of 170.3 and 172.3 GeV. In this paper direct searches for $\tilde{t}_1$ and $\tilde{b}_1$ using the data collected with the OPAL detector at these centre-of-mass energies are reported. The results reported here have been obtained by combining the results obtained at these two new centre-of-mass energies with those obtained at $\sqrt{s}$ = 130, 136 and 161 GeV [8].

In this paper the phenomenology of the production and decay of the $\tilde{t}_1$ ($\tilde{b}_1$) is described in section 2 and the OPAL detector and the event simulation for signal and background processes are given in section 3. In section 4 the data analysis is described and the results are given in section 5.

2 Production and Decay of $\tilde{t}_1$ and $\tilde{b}_1$

Scalar top quark pairs, $\tilde{t}_1\bar{\tilde{t}}_1$, could be produced in e^+e^- annihilation via a virtual Z^0 boson or a virtual photon. The coupling between the $\tilde{t}_1$ and the Z^0 boson depends on a mixing angle, $\theta_{\tilde{t}}$, which is defined by $\tilde{t}_1 = \tilde{t}_L \cos\theta_{\tilde{t}} + \tilde{t}_R \sin\theta_{\tilde{t}}$. This mixing angle is determined by the top quark mass and the soft SUSY breaking parameters [2]. One virtue of the scalar top (scalar bottom) search is that the production cross section depends only on the mass of the scalar top (scalar bottom) and the mixing angle in which all the soft SUSY breaking parameters are hidden. For $\theta_{\tilde{t}}$ close to 0.98 radian ($\cos^2\theta_{\tilde{t}} = \frac{4}{3}\sin^2\overline{\theta}_W$, where $\overline{\theta}_W$ is the effective weak mixing angle), $\tilde{t}_1$ decouples from the Z^0 boson, and $\tilde{t}_1\bar{\tilde{t}}_1$ can be produced only via a virtual γ. The differential cross section $d\sigma/d\cos\theta$ is proportional to $\sin^2\theta$, where θ is the polar angle between the $\tilde{t}_1$ momentum direction and the beam axis, since the spinless $\tilde{t}_1$ is pair produced through a virtual Z^0 boson or a virtual photon.

The following three decay modes are possible for the $\tilde{t}_1$.

(1) $\tilde{t}_1 \to c\tilde{\chi}^0_1$: This 2-body decay would occur via one-loop processes, and the decay width of this mode is estimated to be [2]

$$\Gamma(\tilde{t}_1 \to c\tilde{\chi}^0_1) = (0.3 \sim 3) \times 10^{-10}\, m_{\tilde{t}_1} \left(1 - \frac{{m_{\tilde{\chi}^0_1}}^2}{{m_{\tilde{t}_1}}^2}\right)^2 \quad .$$

(2) $\tilde{t}_1 \to b\ell^+\tilde{\nu}$: If the scalar neutrino $\tilde{\nu}$ is lighter than $(m_{\tilde{t}_1} - m_b - m_{\ell^\pm})$, this 3-body decay would occur as follows: the $\tilde{t}_1$ decays into a b-quark and a virtual state of the chargino $\tilde{\chi}^+_1$, which decays into ℓ^+ plus $\tilde{\nu}$. Since a $\tilde{\nu}$ lighter than 37.1 GeV has been excluded at 95% C.L. [9, 10], this decay mode is permitted only for a $\tilde{t}_1$ heavier than about 42 GeV. The branching fraction to each lepton flavour ℓ^+ depends on the composition of the intermediate chargino. As the chargino becomes Higgsino-like, the branching fraction

into $b\tau^+\tilde{\nu}_\tau$ becomes large. In the limit that the chargino is the pure Wino state, the branching fraction to each lepton flavour is the same. Two cases in which the branching fraction to each lepton flavour is the same, or the branching fraction into $b\tau^+\tilde{\nu}_\tau$ is 100%, were considered in this analysis. This decay process is suppressed by the propagator effect of the heavy $\tilde{\chi}_1^\pm$, and the decay width strongly depends on the masses of $\tilde{\chi}_1^\pm$ and $\tilde{t}_1$. The width of this 3-body decay is estimated to be [2]

$$\Gamma(\tilde{t}_1 \to b\ell^+\tilde{\nu}) = (0.1 \sim 10) \times 10^{-7}\, m_{\tilde{t}_1} \left(\frac{m_{\tilde{t}_1}}{100\mathrm{GeV}}\right)^4 \left(\frac{M_W}{m_{\tilde{\chi}_1^\pm}}\right)^4 \quad ,$$

where M_W is the mass of the W boson. There is large uncertainty on this width due to the coupling strength of $\tilde{t}_1$-$\tilde{\chi}_1^+$-b, but this decay width is much larger than $\Gamma(\tilde{t}_1 \to c\tilde{\chi}_1^0)$, if $m_{\tilde{\chi}_1^\pm}$ is smaller than 200 GeV.

(3) $\tilde{t}_1 \to b\tilde{\chi}_1^0 f_1 \bar{f}_2$: This 4-body decay would, for example, occur as follows: the $\tilde{t}_1$ decays into a b-quark and a virtual state of the chargino $\tilde{\chi}_1^+$, which decays into $\tilde{\chi}_1^0$ and a virtual W^+. However this process is kinematically suppressed by both $\tilde{\chi}_1^\pm$- and $W^\pm$-propagators, and its decay width is estimated to be [2]

$$\Gamma(\tilde{t}_1 \to b\tilde{\chi}_1^0 f_1 \bar{f}_2) = \mathcal{O}(10^{-13})\, m_{\tilde{t}_1} \quad ,$$

when $m_{\tilde{\chi}_1^\pm}$ is about 100 GeV. This width is much smaller than $\Gamma(\tilde{t}_1 \to c\tilde{\chi}_1^0)$, and can be neglected.

For the $m_{\tilde{t}_1}$ range within the reach of LEP2, the decay widths of these modes are estimated to be $\Gamma(\tilde{t}_1 \to c\tilde{\chi}_1^0) = \mathcal{O}(10\,\mathrm{eV})$, $\Gamma(\tilde{t}_1 \to b\ell^+\tilde{\nu}) = \mathcal{O}(10\,\mathrm{keV})$ and $\Gamma(\tilde{t}_1 \to b\tilde{\chi}_1^0 f_1 \bar{f}_2) = \mathcal{O}(0.01\,\mathrm{eV})$. The dominant decay mode is therefore $\tilde{t}_1 \to b\ell^+\tilde{\nu}$, if it is kinematically allowed. Otherwise the flavour changing two-body decay, $\tilde{t}_1 \to c\tilde{\chi}_1^0$, is dominant. Because the lifetime of the $\tilde{t}_1$ is much larger than the typical time scale of hadronisation, the $\tilde{t}_1$ would form a $\tilde{t}_1$-hadron before it decays. However, the decay length of the $\tilde{t}_1$ is sufficiently small that the $\tilde{t}_1$-hadron decays close to the interaction point.

Scalar bottom quark pairs, $\tilde{b}_1\bar{\tilde{b}}_1$, could also be produced in the same way as $\tilde{t}_1\bar{\tilde{t}}_1$. Since the $\tilde{b}_1$ is a mixed state of $\tilde{b}_L$ and $\tilde{b}_R$, *i.e.* $\tilde{b}_1 = \tilde{b}_L \cos\theta_{\tilde{b}} + \tilde{b}_R \sin\theta_{\tilde{b}}$, the production cross-section depends on this mixing angle. For $\theta_{\tilde{b}}$ close to 1.167 radian ($\cos^2\theta_{\tilde{b}} = \frac{2}{3}\sin^2\overline{\theta}_W$), the $\tilde{b}_1$ decouples from the Z^0 boson, and $\tilde{b}_1\bar{\tilde{b}}_1$ can be produced only via a virtual γ.

Assuming that the second lightest neutralino, $\tilde{\chi}_2^0$, is heavier than the $\tilde{b}_1$, the dominant decay mode of $\tilde{b}_1$ is restricted [2] to be $\tilde{b}_1 \to b\tilde{\chi}_1^0$. The width of this decay mode is estimated to be [4]:

$$\Gamma(\tilde{b}_1 \to b\tilde{\chi}_1^0) \sim 10^{-3}\, m_{\tilde{b}_1} \left(1 - \frac{{m_{\tilde{\chi}_1^0}}^2}{{m_{\tilde{b}_1}}^2}\right)^2 \quad .$$

As for the $\tilde{t}_1$, the lifetime of the $\tilde{b}_1$ is larger than the typical time scale of hadronisation, and the $\tilde{b}_1$ would form a $\tilde{b}_1$-hadron before it decays.

[2] If $\tilde{\chi}_2^0$ is lighter than $\tilde{b}_1$ and the $\tilde{b}_L$-component of $\tilde{b}_1$ is large, the dominant decay mode of $\tilde{b}_1$ would be $\tilde{b}_1 \to b\tilde{\chi}_2^0$. Also the $\tilde{b}_1 \to c\tilde{\chi}_1^-$ decay is not considered, because a $\tilde{\chi}_1^\pm$ lighter than 80 GeV is not favoured [11].

3 The OPAL Detector and Event Simulation

3.1 The OPAL Detector

The OPAL detector, which is described in detail in ref. [12], is a multipurpose apparatus having nearly complete solid angle coverage. The central detector consists of a silicon strip detector and tracking chambers, providing charged particle tracking for over 96% of the full solid angle, inside a uniform solenoidal magnetic field of 0.435 T. A lead-glass electromagnetic (EM) calorimeter located outside the magnet coil is hermetic in the polar angle range [3] of $|\cos\theta| < 0.82$ for the barrel region and $0.81 < |\cos\theta| < 0.984$ for the endcap region. The magnet return yoke consisting of barrel and endcap sections along with pole tips is instrumented for hadron calorimetry (HCAL) in the region $|\cos\theta| < 0.99$. Four layers of muon chambers cover the outside of the hadron calorimeter. Calorimeters close to the beam axis measure the luminosity using small angle Bhabha scattering events and complete the geometrical acceptance down to 24 mrad. These include the forward detectors (FD) which are lead-scintillator sandwich calorimeters and, at smaller angles, silicon tungsten calorimeters (SW) [13] located on both sides of the interaction point. The gap between the endcap EM calorimeter and the FD is filled by an additional lead-scintillator electromagnetic calorimeter, called the gamma-catcher.

3.2 Monte Carlo Event Simulation of $\tilde{\mathrm{t}}_1$ and $\tilde{\mathrm{b}}_1$

Monte Carlo simulation of the production and decay of the $\tilde{\mathrm{t}}_1$ was performed as follows. The $\tilde{\mathrm{t}}_1\bar{\tilde{\mathrm{t}}}_1$ pairs were generated taking into account initial state radiation [14]. The hadronisation process was subsequently performed to produce colourless $\tilde{\mathrm{t}}_1$-hadrons and other fragmentation products according to the Lund string fragmentation scheme (JETSET 7.4) [14, 15]. The parameters for perturbative QCD and fragmentation processes have been optimised using event shape distributions of the hadronic Z^0 decays measured by OPAL [16]. For the fragmentation of the $\tilde{\mathrm{t}}_1$, the fragmentation function proposed by Peterson *et al.* [14, 17] was used, where the parameter $\epsilon_{\tilde{\mathrm{t}}_1}$ was set to

$$\epsilon_{\tilde{\mathrm{t}}_1} = \epsilon_{\mathrm{b}} m_{\mathrm{b}}^2 / m_{\tilde{\mathrm{t}}_1}^2 \quad (\epsilon_{\mathrm{b}} = 0.0038\ [16],\ m_{\mathrm{b}} = 5\ \mathrm{GeV}) \ . \tag{1}$$

The $\tilde{\mathrm{t}}_1$-hadron was formed from a $\tilde{\mathrm{t}}_1$ and a spectator quark or diquark [18]. The fragmentation products excluding the $\tilde{\mathrm{t}}_1$-hadrons carry less than 2% of the centre-of-mass energy. For the $\tilde{\mathrm{t}}_1$ decaying into $\mathrm{c}\tilde{\chi}_1^0$, a colour string was stretched between the charm quark and the spectator. This colour singlet system was hadronised using the Lund scheme [14, 15]. Gluon bremsstrahlung (QCD parton showering) was allowed in this process, and the Peterson function was also used for the charm quark fragmentation, where ϵ_{c} was set to 0.031 [16].

The signals for the decays $\tilde{\mathrm{t}}_1 \to \mathrm{b}\ell^+\tilde{\nu}$ and $\tilde{\mathrm{b}}_1 \to \mathrm{b}\tilde{\chi}_1^0$ were also generated in a similar manner. The $\tilde{\mathrm{t}}_1\bar{\tilde{\mathrm{t}}}_1$ events, in which the $\tilde{\mathrm{t}}_1$ decays into $\mathrm{c}\tilde{\chi}_1^0$, were generated for 56 combinations of $(m_{\tilde{\mathrm{t}}_1}, m_{\tilde{\chi}_1^0})$. The $\tilde{\mathrm{t}}_1\bar{\tilde{\mathrm{t}}}_1$ ($\tilde{\mathrm{t}}_1 \to \mathrm{b}\ell^+\tilde{\nu}$ and $\tilde{\mathrm{t}}_1 \to \mathrm{b}\tau^+\tilde{\nu}$) events were generated for 48 combinations of $(m_{\tilde{\mathrm{t}}_1}, m_{\tilde{\nu}})$, and the $\tilde{\mathrm{b}}_1\bar{\tilde{\mathrm{b}}}_1$ events for 48 combinations of $(m_{\tilde{\mathrm{b}}_1}, m_{\tilde{\chi}_1^0})$. At each point 1000 events

[3] A right-handed coordinate system is adopted, where the x-axis points to the centre of the LEP ring, and positive z is along the electron beam direction. The angles θ and ϕ are the polar and azimuthal angles, respectively.

were generated at a centre-of-mass energy of $\sqrt{s} = 171$ GeV. The mixing angles of the $\tilde{t}_1$ and $\tilde{b}_1$ were set to zero when these events were generated. The dependence of the detection efficiencies on these mixing angles will be discussed in section 5.1. The generated events were processed through the full simulation of the OPAL detector [19], and the same event analysis chain was applied to the simulated events and the data.

3.3 Monte Carlo Event Simulation of Background Processes

The background processes were simulated as follows:

• Two-photon processes are the most important background for the case of a small mass difference Δm ($\equiv m_{\tilde{t}_1} - m_{\tilde{\chi}^0_1}$, $m_{\tilde{t}_1} - m_{\tilde{\nu}}$, or $m_{\tilde{b}_1} - m_{\tilde{\chi}^0_1}$), since such signal events have small visible energy and small transverse momentum relative to the beam direction. Using the Monte Carlo generators PYTHIA [14], PHOJET [20] and HERWIG [21] hadronic events from two-photon processes were simulated in which the invariant mass of the photon-photon system ($M_{\gamma\gamma}$) was larger than 2.5 GeV. Monte Carlo samples for four-lepton events ($e^+e^-e^+e^-$, $e^+e^-\mu^+\mu^-$ and $e^+e^-\tau^+\tau^-$) were generated with the Vermaseren program [22].

• τ pairs, in which one of the τ decays into a low momentum electron and energetic neutrinos, are a background to acoplanar two-jet events. The KORALZ event generator [23] was used for the generation of $\tau^+\tau^-(\gamma)$ and $\mu^+\mu^-(\gamma)$ events. The BHWIDE program [24] was used for $e^+e^- \to e^+e^-(\gamma)$ events.

• Multijet hadronic events $e^+e^- \to q\bar{q}(\gamma)$ in which one or two jet momenta are mismeasured are the significant background for the large Δm region ($\gtrsim m_{\tilde{t}_1}/2$ or $m_{\tilde{b}_1}/2$). The PYTHIA generator was used to simulate hadronic events.

• Finally, four-fermion processes in which at least one of the fermions is a neutrino constitute a serious background. The dominant contributions come from W^+W^- or γ^*Z^0 events. Since the interference effects of various diagrams are important, the grc4f generator [25] was used, which takes into account all interfering diagrams and includes initial state photon radiation.

These background events were also processed through the full simulation, and the same event analysis chain as used for the data was applied to these simulated events.

4 Analysis

The present analysis is based on the data collected during the autumn 1996 run of LEP. The data used in this analysis correspond to an integrated luminosity of 1.0 and 9.4 pb^{-1} at centre-of-mass energies of $\sqrt{s}$ =170.3 and 172.3 GeV, respectively. Since the event topologies of $\tilde{t}_1 \to c\tilde{\chi}^0_1$ and $\tilde{b}_1 \to b\tilde{\chi}^0_1$ are very similar, the same selection criteria were used for these modes (section 4.1 analysis A). In section 4.2 (analysis B), the selection criteria for $\tilde{t}_1 \to b\ell^+\tilde{\nu}$ are discussed. These analyses are very similar to those in ref. [8].

To select good tracks and clusters, the same quality criteria as in ref. [8] were used except that the transverse momentum of each track was required to be larger than 120 MeV. Variables used for the cuts, like the total visible energy, $E_{\rm vis}$, the total transverse momentum and the acoplanarity angle (defined below) were calculated as follows. First the four-momenta of the tracks and those of the EM and HCAL clusters not associated with charged tracks were summed.

Whenever a calorimeter cluster had associated charged tracks, the expected energy deposited by the tracks was subtracted from the cluster energy to reduce double counting. If the energy of a cluster was smaller than the expected energy deposited by the associated tracks, the cluster energy was not used. Hadron calorimeter clusters were also used in calculating event variables. In the case of the transverse momentum and the visible mass, the values calculated without the HCAL clusters were also used.

The following preselection criteria (P1 – P4), which are common to both analyses A and B, were applied first. The numbers of events remaining after each cut are listed in Table 1. For comparison, the table also shows the corresponding numbers of simulated events for background processes and for three samples of the simulated $\tilde{\mathrm{t}}_1\bar{\tilde{\mathrm{t}}}_1$ ($\tilde{\mathrm{t}}_1 \to \mathrm{c}\tilde{\chi}^0_1$) and $\tilde{\mathrm{b}}_1\bar{\tilde{\mathrm{b}}}_1$ events.

(P1) The number of charged tracks was required to be at least four. The ratio of the number of good tracks to the total number of reconstructed tracks was required to be greater than 0.2 in order to reduce beam-gas and beam-wall background events. The visible mass of the event, excluding the hadron calorimeter, was also required to be larger than 2.5 GeV, since the hadronic two-photon processes were only simulated for $M_{\gamma\gamma} \geq 2.5$ GeV.

(P2) To reduce the background from two-photon processes and multihadronic events, where a jet axis was close to the beam direction, the total energy deposited had to be less than 5 GeV in each SW detector, less than 2 GeV in each FD detector and less than 5 GeV in each side of the gamma-catcher. In addition, the visible energy in the region of $|\cos\theta| > 0.9$ was required to be less than 20% of the total visible energy.

(P3) The polar angle of the missing momentum direction, θ_{miss}, was required to satisfy $|\cos\theta_{\mathrm{miss}}| < 0.9$.

(P4) Events from two-photon processes were eliminated from the data by demanding that the event transverse momentum excluding the hadron calorimeter, P_t, be greater than 5 GeV and that the transverse momentum including the hadron calorimeter, P_t^{HCAL}, be greater than 6 GeV. Fig. 1 shows the distribution of P_t just before these cuts.

4.1 Analysis A: $\tilde{\mathrm{t}}_1 \to \mathrm{c}\tilde{\chi}^0_1$ and $\tilde{\mathrm{b}}_1 \to \mathrm{b}\tilde{\chi}^0_1$

The experimental signature for $\tilde{\mathrm{t}}_1\bar{\tilde{\mathrm{t}}}_1(\tilde{\mathrm{t}}_1 \to \mathrm{c}\tilde{\chi}^0_1)$ events and $\tilde{\mathrm{b}}_1\bar{\tilde{\mathrm{b}}}_1$ events is an acoplanar two-jet topology with a large transverse momentum with respect to the beam axis. The fragmentation functions of $\tilde{\mathrm{t}}_1$ and $\tilde{\mathrm{b}}_1$ are very hard, therefore the jets are expected to be narrow.

The event selection criteria are described below. Figs. 2–4 show the distributions of the main cut variables at various stages of applying the cuts. The numbers of events remaining after each cut are also listed in Table 1.

(A1) The number of reconstructed jets was required to be exactly two. Jets were reconstructed using the Durham algorithm [26] with the jet resolution parameter of $y_{cut} = 0.005/(E_{\mathrm{vis}}/\sqrt{s})$. This E_{vis}-dependence of the y_{cut} parameter was necessary for good jet-reconstruction over a wide range of $m_{\tilde{\mathrm{t}}_1}$, $m_{\tilde{\mathrm{b}}_1}$ and $m_{\tilde{\chi}^0_1}$. Fig. 2 shows the number of reconstructed jets before this cut.

(A2) Both reconstructed jets were required to contain at least two charged particles to reduce the $\tau^+\tau^-$ background where at least one of the τ decayed into only one charged particle.

(A3) The arithmetic mean of the invariant masses of the jets, $\bar{M}_{\rm jet}$, was required to be smaller than 8 GeV. When the invariant mass of the event, $M_{\rm vis}$, was within $\pm$15 GeV of the W-boson mass, a harder cut on $\bar{M}_{\rm jet}$ was applied to reduce the Weν background events: $\bar{M}_{\rm jet} < 4$ GeV. Fig. 3 shows the scatter plots of $M_{\rm vis}$-$\bar{M}_{\rm jet}$ for real data, the Monte Carlo events for the multihadron, the lepton-pair, the four-fermion processes and the $\tilde{\rm t}_1\bar{\tilde{\rm t}}_1$ events. As shown in Fig. 3(e) and 3(f), jets from the $\tilde{\rm t}_1$ are expected to have low invariant masses, because the fragmentation function of the $\tilde{\rm t}_1$ is hard and only a few particles are emitted from the fragmentation process of $\tilde{\rm t}_1\bar{\tilde{\rm t}}_1$.

(A4) The acoplanarity angle, $\phi_{\rm acop}$, was defined as $\pi - \phi_{\rm open}$, where $\phi_{\rm open}$ is the azimuthal opening angle between the directions of the two reconstructed jets. To ensure the reliability of the calculation of $\phi_{\rm acop}$, both jet axes were required to be more than 20° away from the beam axis. The value of $\phi_{\rm acop}$ was required to be greater than 20°. Fig. 4 shows the distributions of $\phi_{\rm acop}$ just before this selection.

After all the cuts, no events were observed in the data, which is consistent with the number of expected background events of 0.44. The efficiencies for $\tilde{\rm t}_1\bar{\tilde{\rm t}}_1$ and $\tilde{\rm b}_1\bar{\tilde{\rm b}}_1$ events are listed in Tables 2 and 3. Both efficiencies were 30–60%, if the mass difference between the $\tilde{\rm t}_1(\tilde{\rm b}_1)$ and $\tilde{\chi}^0_1$ was larger than 10 GeV. A modest efficiency of about 20% was also obtained for a mass difference of 5 GeV for $\tilde{\rm t}_1\bar{\tilde{\rm t}}_1$ events. In addition to effects included in the detector simulation, an additional efficiency loss of 2% (relative) arose from beam-related background in the silicon-tungsten calorimeter, estimated using random beam crossing events. The efficiencies given in Tables 1–5 do not include this correction, but it is included when deriving the mass limits.

	data	total bkg.	$q\bar{q}(\gamma)$	$\ell^+\ell^-(\gamma)$	'$\gamma\gamma$'	4-f	$\tilde{\rm t}_1\bar{\tilde{\rm t}}_1$ and $\tilde{\rm b}_1\bar{\tilde{\rm b}}_1$		
$m_{\tilde{\rm t}_1}$ (GeV)							70	70	–
$m_{\tilde{\rm b}_1}$ (GeV)							–	–	70
$m_{\tilde{\chi}^0_1}$ (GeV)							60	35	50
Presel. 1	51455	50466	1105	291.9	48948	120.7	942	934	988
Presel. 2	10395	9949	581	75.2	9200	92.8	814	798	874
Presel. 3	4851	4712	245	59.0	4326	82.7	752	741	812
Presel. 4	268	246	143	35.1	3.27	65.2	650	729	764
cut (A1)	125	101	62.0	31.3	2.39	5.58	588	688	701
cut (A2)	80	69.3	61.7	2.33	0.950	4.40	515	637	684
cut (A3)	5	4.63	1.45	2.05	0.696	0.430	514	546	652
cut (A4)	0	0.440	0.006	0.009	0.085	0.340	476	501	581

Table 1: The remaining numbers of events normalised to the integrated luminosity of the data for various background processes are compared with data after each cut. Numbers for three simulated event samples of $\tilde{\rm t}_1\bar{\tilde{\rm t}}_1$ and $\tilde{\rm b}_1\bar{\tilde{\rm b}}_1$ are also given (starting from 1000 events for each).

$m_{\tilde{t}_1}$ (GeV)	45	47	50	55	60	65	70	75
Δm								
3.0 GeV	8	8	7	6	4	3	3	1
5.0 GeV	28	27	27	26	24	24	19	19
10.0 GeV	41	42	44	45	46	44	48	48
20.0 GeV	39	43	44	47	52	52	53	58
$m_{\tilde{t}_1}/2$	40	40	40	45	43	45	50	52
$m_{\tilde{t}_1}-10$ GeV	36	36	36	38	36	40	37	43
$m_{\tilde{t}_1}$	38	34	36	37	34	39	36	38

Table 2: The detection efficiencies in percent for $\tilde{t}_1\bar{\tilde{t}}_1$, in which $\tilde{t}_1$ decays into $c\tilde{\chi}_1^0$ for different $\tilde{t}_1$ masses and Δm values, where Δm is $m_{\tilde{t}_1} - m_{\tilde{\chi}_1^0}$.

$m_{\tilde{b}_1}$ (GeV)	45	47	50	55	60	65	70	75
Δm								
7.0 GeV	22	23	23	25	23	23	22	23
10.0 GeV	40	40	43	44	48	48	49	48
20.0 GeV	40	41	45	49	53	57	58	63
$m_{\tilde{b}_1}/2$	36	35	38	41	42	46	49	53
$m_{\tilde{b}_1}-10$ GeV	32	32	31	33	34	37	34	42
$m_{\tilde{b}_1}$	32	32	32	31	33	35	35	41

Table 3: The detection efficiencies in percent for $\tilde{b}_1\bar{\tilde{b}}_1$ for different $\tilde{b}_1$ masses and Δm values, where $\Delta m = m_{\tilde{b}_1} - m_{\tilde{\chi}_1^0}$.

4.2 Analysis B: $\tilde{t}_1 \to b\ell\tilde{\nu}$

The experimental signature for $\tilde{t}_1\bar{\tilde{t}}_1(\tilde{t}_1 \to b\ell\tilde{\nu})$ events is an acoplanar two-jet plus two-lepton topology with a missing transverse momentum with respect to the beam axis. A large missing energy is also expected for this decay mode, since a $\tilde{\nu}$ lighter than 37.1 GeV has already been excluded at 95% C.L. by LEP1 data [9, 10]. The numbers of events remaining after each cut are listed in Table 4. For comparison, the table also shows the corresponding numbers for simulated events for background processes and for three samples of simulated $\tilde{t}_1\bar{\tilde{t}}_1$ events, in which the branching fraction to each lepton flavour is assumed to be the same. Figs. 5 – 7 show the distributions of the main cut variables at various stages of applying selection cuts.

(B1) The number of charged tracks was required to be at least six.

(B2) The number of reconstructed jets was required to be at least four, because the signal should contain two hadronic jets plus two isolated leptons. Jets were reconstructed using the Durham algorithm [26] with the jet resolution parameter [4] of $y_{\rm cut} = 0.004$. Fig. 5 shows the distributions of the number of reconstructed jets just before this selection.

(B3) A candidate event was required to contain at least one lepton, if the total visible energy normalised to the centre-of-mass energy, $E_{\rm vis}/\sqrt{s}$, was larger than 0.3. Leptons were

[4] A constant $y_{\rm cut}$ parameter was used in order to find efficiently jets from τ-decay.

identified in the following way: Electrons were selected if they satisfied either of the two identification methods described in ref. [27], and muons were identified using the two methods described in ref. [28]. The track momentum of the electron or muon candidate was required to be larger than 5 GeV. A jet reconstructed in cut (B2) was identified as a tau decay if only one or three charged tracks appeared in the jet, the invariant mass of the charged particles in the jet was smaller than 1.5 GeV, the invariant mass including energies deposited in the calorimeters was smaller than 2 GeV and the scalar sum of momenta of the charged tracks was larger than 5 GeV.

(B4) The total visible energy normalised to the centre-of-mass energy, $E_{\rm vis}/\sqrt{s}$, was required to be smaller than 0.55, since much of the energy would be carried by two $\tilde{\nu}$'s as mentioned before. As shown in Fig. 6, a large fraction of $\rm W^+W^-$ and multihadronic background events were rejected.

(B5) The visible mass of the events, $M_{\rm vis}$, must be smaller than 70 GeV in order to reduce $\rm W^+W^-$ background events in which one of $\rm W^{\pm}$'s decayed into $\tau\nu$ and the other $\rm W^{\pm}$ decayed into $\rm q\bar{q}^{'}(g)$.

(B6) In order to examine the acoplanarity of the events, jets were reconstructed using the Durham algorithm where the number of jets was forced to be two. To ensure the reliability of the calculation of the acoplanarity angle, both jets were required to be more than 20° away from the beam axis. Finally, the acoplanarity angle between these two jets was required to be greater than 15°. Fig. 7 shows the distribution of $\phi_{\rm acop}$ just before this cut. In the three-body decay, the transverse momentum carried by the $\tilde{\nu}$ with respect to the original $\tilde{\rm t}_1$-momentum is smaller than that of $\tilde{\chi}^0_1$ in the two-body decay. When the $\tilde{\rm t}_1$ is light, the outgoing $\tilde{\nu}$ is strongly boosted toward the direction of the parent $\tilde{\rm t}_1$. Hence $\phi_{\rm acop}$ for the signal would become small. This is the reason for the use of a looser $\phi_{\rm acop}$ cut.

No events were observed in the data after the above cuts. The number of expected background events was 0.17. The detection efficiencies for $\tilde{\rm t}_1\bar{\tilde{\rm t}}_1$ events are listed in Table 5. As shown in this table, the detection efficiencies for $\tilde{\rm t}_1 \to {\rm b}\tau^+\tilde{\nu}_\tau$ are slightly smaller than the case of the same branching fraction to each lepton flavour, if the mass difference is smaller than 10 GeV.

5 Results

No evidence for $\tilde{\rm t}_1\bar{\tilde{\rm t}}_1$ and $\tilde{\rm b}_1\bar{\tilde{\rm b}}_1$ pair-production was observed in the data. The data were consistent with the expected background of 0.44 events in analysis A and 0.17 events in analysis B for the integrated luminosity of 10.4 $\rm pb^{-1}$. Therefore lower limits on $m_{\tilde{\rm t}_1}$ and $m_{\tilde{\rm b}_1}$ were calculated. The results obtained at lower centre-of-mass energies ($\sqrt{s}$ = 130, 136 and 161 GeV) [8] were included in calculating these limits.

5.1 Systematic Errors

The following sources of systematic error on the expected number of the signal events were taken into account:

	data	total bkg.	$q\bar{q}(\gamma)$	$\ell^+\ell^-(\gamma)$	'$\gamma\gamma$'	4-f	$\tilde{t}_1\bar{\tilde{t}}_1$		
$m_{\tilde{t}_1}$ (GeV)							50	70	70
$m_{\tilde{\nu}}$ (GeV)							35	55	35
Presel.	268	246	143	35.1	3.27	65.2	706	670	741
cut (B1)	224	210	143	2.80	1.20	63.8	706	670	740
cut (B2)	59	56.8	22.7	0.055	0.338	33.8	541	619	537
cut (B3)	17	17.8	4.05	0.052	0.338	13.3	527	619	510
cut (B4)	1	1.06	0.173	0.003	0.338	0.547	527	619	507
cut (B5)	1	0.500	0.096	0.001	0.338	0.065	523	619	427
cut (B6)	0	0.171	0.038	0.000	0.085	0.048	380	528	358

Table 4: The remaining numbers of events normalised to the integrated luminosity of the data for various background processes are compared with data after each cut. Numbers for three simulated event samples of $\tilde{t}_1\bar{\tilde{t}}_1$ are also given (starting from 1000 events for each). In these samples, the branching fraction to each lepton flavour is assumed to be the same.

1. There is an error of 0.06 GeV [29] on the reported centre-of-mass energies. The production cross-sections of the $\tilde{t}_1\bar{\tilde{t}}_1$ and $\tilde{b}_1\bar{\tilde{b}}_1$ were calculated conservatively at $\sqrt{s} = 170.2$ and 172.2 GeV, which energies were reduced by one standard deviation from 170.3 and 172.3 GeV, respectively.

2. The statistical error of the signal Monte Carlo simulation is estimated to be 2–10% depending on detection efficiencies.

3. The dependence of the detection efficiency on the mixing angle:
   The energy distribution of the initial state radiation depends on the mixing angle of the $\tilde{t}_1$ ($\tilde{b}_1$), because it influences the coupling between the $\tilde{t}_1$ ($\tilde{b}_1$) and the Z^0. The detection efficiencies therefore depend on $\theta_{\tilde{t}}$ ($\theta_{\tilde{b}}$). However, the detection efficiencies in Tables 2, 3 and 5 were calculated using the simulated events which were generated for $\theta_{\tilde{t}} = \theta_{\tilde{b}} = 0.0$.
   The detection efficiencies in the two extreme cases of $\tilde{t}_1$ decoupled from the Z^0 ($\theta_{\tilde{t}} = 0.98$) and $\tilde{t}_1 = \tilde{t}_L$ ($\theta_{\tilde{t}} = 0.0$) were compared for various $m_{\tilde{t}_1}$ values. The difference was always found to be within 2–4%. The range is due to the different values of $m_{\tilde{t}_1}$, and this difference was taken to be a systematic error. The effect on efficiencies for $\tilde{t}_1 \to b\ell\tilde{\nu}$ and $\tilde{b}_1 \to b\tilde{\chi}^0_1$ was also checked and similar results were obtained.

4. Fragmentation function for $\tilde{t}_1$:
   The fragmentation scheme proposed by Peterson *et al.* was used, with the fragmentation parameter $\epsilon_{\tilde{t}_1}$ determined by equation (1). The error on $\epsilon_{\tilde{t}_1}$ was propagated from $\delta\epsilon_b/\epsilon_b = \pm 0.26$ [16] and $\delta m_b/m_b = \pm 0.06$ [10], corresponding to $\delta\epsilon_{\tilde{t}_1}/\epsilon_{\tilde{t}_1} = \pm 0.27$. The systematic error in the efficiencies due to this uncertainty was evaluated by altering the $\epsilon_{\tilde{t}_1}$ parameter by one standard deviation for several combinations of ($m_{\tilde{t}_1}$, $m_{\tilde{\chi}^0_1}$) and ($m_{\tilde{t}_1}$, $m_{\tilde{\nu}}$). For the $\tilde{t}_1 \to c\tilde{\chi}^0_1$ mode, the detection efficiencies changed by no more than 5% over the $m_{\tilde{t}_1}$ range. The relative changes for $\tilde{t}_1 \to b\ell\tilde{\nu}$ mode were found to be 4–10%, and they depended mainly on $m_{\tilde{t}_1}$.

$\tilde{t}_1 \to b\ell\tilde{\nu}$, ℓ= e, μ, τ the same branching fraction								
$m_{\tilde{t}_1}$ (GeV)	45	47	50	55	60	65	70	75
Δm								
7.0 GeV	8	7	8	9	8	7	8	6
10.0 GeV	26	25	30	32	34	34	35	36
15.0 GeV	29	35	38	44	49	53	53	55
20.0 GeV	29	32	30	41	46	50	52	55
$m_{\tilde{t}_1}/2$	34	33	31	37	39	39	36	37

$\tilde{t}_1 \to b\tau\tilde{\nu}_\tau$, 100% branching fraction								
$m_{\tilde{t}_1}$ (GeV)	45	47	50	55	60	65	70	75
Δm								
7.0 GeV	2	3	2	1	0	0	0	0
10.0 GeV	20	20	22	25	25	28	25	26
15.0 GeV	27	32	37	43	47	54	54	53
20.0 GeV	29	31	30	36	46	52	55	56
$m_{\tilde{t}_1}/2$	34	33	34	37	38	39	39	38

Table 5: The detection efficiencies in percent for $\tilde{t}_1\bar{\tilde{t}}_1$, in which $\tilde{t}_1$ decays into $b\ell\tilde{\nu}$ ($\ell = e, \mu, \tau$). The upper half of the table shows the case that the branching fraction to each lepton flavour is the same and the lower half shows the worst case that the branching fraction of $\tilde{t}_1 \to b\tau\tilde{\nu}_\tau$ is 100%. In both tables, Δm is defined as $m_{\tilde{t}_1} - m_{\tilde{\nu}}$.

To estimate the dependence on the fragmentation scheme, the fragmentation function proposed by Bowler [30] was used, because the shape of this fragmentation function is very different from that of Peterson. The relative difference in efficiencies between the two fragmentation models was 2–3% for the $\tilde{t}_1 \to c\tilde{\chi}_1^0$ mode, which was smaller than that due to the variation of the $\epsilon_{\tilde{t}_1}$ parameter used in the Peterson fragmentation scheme. The systematic error due to the dependence on the fragmentation model was taken to be 3%. For the $\tilde{t}_1 \to b\ell\tilde{\nu}$ mode, the relative difference in efficiencies was found to lie between 4–11%, where the range was mainly due to $m_{\tilde{t}_1}$.

5. Fragmentation function for $\tilde{b}_1$:
   The error due to the fragmentation function for $\tilde{b}_1$ was also estimated using the methods described above. The uncertainty in $\epsilon_{\tilde{b}_1}$ made a relative difference of 4–7% in the efficiencies.

6. Fragmentation of the charm and bottom quarks:
   The error in the efficiencies for the $\tilde{t}_1 \to c\tilde{\chi}_1^0$ mode due to the ambiguity in ϵ_c was estimated to be typically 3% by changing ϵ_c by $\delta\epsilon_c/\epsilon_c = \pm\ 0.35$ [16].

   The uncertainty in the ϵ_b parameter also contributes to the error in the efficiencies for the $\tilde{t}_1 \to b\ell\tilde{\nu}$ and $\tilde{b}_1 \to b\tilde{\chi}_1^0$ modes. As mentioned above, the ϵ_b parameter was simultaneously changed by $\pm$26% when $\epsilon_{\tilde{t}_1}$ and $\epsilon_{\tilde{b}_1}$ were altered. Therefore the systematic error due to the uncertainty on ϵ_b is taken into account in the errors $\delta\epsilon_{\tilde{t}_1}$ and $\delta\epsilon_{\tilde{b}_1}$.

7. Fermi motion of the spectator quark in $\tilde{t}_1$ ($\tilde{b}_1$) -hadron decay:
   Due to the Fermi motion of the spectator quark the invariant mass of the hadronic decay products of a $\tilde{t}_1$ ($\tilde{b}_1$) -hadron varies. For $\tilde{t}_1 \to c\tilde{\chi}^0_1$ and $\tilde{b}_1 \to b\tilde{\chi}^0_1$ modes this effect is not negligible when Δm is large. For the case of a 70 GeV $\tilde{t}_1$ ($\tilde{b}_1$) and a massless neutralino the efficiency varies up to 5% (3%) due to the jet mass cut (A3).

8. Lepton identification:
   The systematic error on electron identification was estimated to be 4% and the error on muon identification was 2%. The systematic error on tau identification is dominated by the uncertainties in the fragmentation of the bottom quark, which has already been included in the uncertainty in the ϵ_b parameter. A conservative error of 4% was applied for all types of leptons.

9. Systematic errors due to imperfections in the Monte Carlo simulation of P_t, the number of reconstructed jets, $E_{\rm vis}$ and $M_{\rm vis}$ were estimated to be 2% [11].

10. The integrated luminosity was calculated using the SW detector. The systematic error on this luminosity was estimated to be $\pm$ 0.4%(stat.) and $\pm$ 0.4%(sys.) [31].

11. The systematic error due to the uncertainty on the trigger efficiency was estimated to be negligible. This is expected because of the requirement of at least four good tracks.

The various systematic errors are summarised in Table 6. These systematic errors were considered to be independent and the total systematic error was calculated as the quadratic sum of the individual errors.

Sources	$\tilde{t}_1 \to c\tilde{\chi}^0_1$	$\tilde{t}_1 \to b\ell\tilde{\nu}$	$\tilde{b}_1 \to b\tilde{\chi}^0_1$
Statistical error of MC	2–10%		
$\theta_{\tilde{t}}$ dependence	2–4%	2–4%	–
$\theta_{\tilde{b}}$ dependence	–	–	2–4%
Uncertainty on $\epsilon_{\tilde{t}_1}$	5%	4–10%	–
Uncertainty on $\epsilon_{\tilde{b}_1}$	–	–	4–7%
Fragmentation scheme	3%	4–11%	3–9%
Uncertainty on ϵ_c	3%	–	–
Uncertainty on ϵ_b	–	Included in the uncertainties of $\epsilon_{\tilde{t}_1}$ and $\epsilon_{\tilde{b}_1}$	
Spectator Fermi motion	0–5%	–	0–3%
Uncertainty of lepton ID	–	4%	–
Detector simulation	2%		
Luminosity	0.6%		
Trigger efficiencies	negligibly small		

Table 6: The summary of the systematic errors on the expected number of the signal events. The errors depend on the mass of $\tilde{t}_1$ and $\tilde{b}_1$.

The systematic errors in the expected number of background events were mostly dominated by the Monte Carlo statistics. For the multihadronic, two-photon and four-fermion processes, the systematic errors in the generators were evaluated as follows.

1. The multihadronic process:
   The expected number of background events using PYTHIA was compared with that obtained with the HERWIG generator. The differences were 0.006 and 0.012 events for analysis A and B, respectively. Although both differences are consistent with zero within the statistical errors, these numbers were treated conservatively as systematic errors.

2. The two-photon processes:
   The uncertainty on the modelling of the two-photon processes was checked with data. In order to select two-photon events the visible energy was required to be smaller than 20% of $\sqrt{s}$, the charged multiplicity to be at least four, the visible invariant mass to be larger than 3 GeV and the forward detector vetoes (cut P2) were required. The P_t distributions of the selected events from data and Monte Carlo were compared after the above cuts. The shapes of the distributions agree with each other, but there is an uncertainty of 30% in the normalisation. This was treated as the systematic error in the prediction of the two-photon background.

3. The four-fermion processes:
   Uncertainties in the generators of four-fermion processes were estimated by comparing grc4f with the Excalibur [32] generator. Since the Weν background events were not generated in Excalibur, the PYTHIA generator was used for this process. The differences were found to be 0.08 and 0.006 events for analyses A and B, respectively.

The total systematic error was calculated as the quadratic sum of these individual errors. The total numbers of background events were expected to be 0.44 ± 0.12 for analysis A and 0.17 ± 0.09 for analysis B. These systematic errors were treated as in ref. [33] in calculating the limits.

5.2 Mass Limits

5.2.1 Scalar top quark $\tilde{t}_1$

In order to calculate mass limits, the number of signal events passing through the event selections is determined as a function of $m_{\tilde{t}_1}$, $m_{\tilde{\chi}^0_1}$ (or $m_{\tilde{\nu}}$) and $\theta_{\tilde{t}}$. Figs. 8(a), 9(a) and 10(a) show the 95% C.L. excluded regions in the ($\theta_{\tilde{t}}$, $m_{\tilde{t}_1}$) plane for the $\tilde{t}_1 \to c\tilde{\chi}^0_1$, $\tilde{t}_1 \to b\ell\tilde{\nu}$ (ℓ= e,μ,τ) and $\tilde{t}_1 \to b\tau\tilde{\nu}$ decay modes, respectively. The 95% C.L. mass bounds are listed in Table 7 for various values of $\theta_{\tilde{t}}$. Assuming that the $\tilde{t}_1$ decays into $c\tilde{\chi}^0_1$, and that the mass difference between the $\tilde{t}_1$ and the $\tilde{\chi}^0_1$ is greater than 10 GeV, the $\tilde{t}_1$ is found to be heavier than 73.3 GeV, if $\theta_{\tilde{t}} = 0$. A lower limit of 65.0 GeV is obtained even if the $\tilde{t}_1$ decouples from the Z^0 boson. When the $\tilde{t}_1$ decays into $b\ell\tilde{\nu}$, the lower limit on $m_{\tilde{t}_1}$ is 67.9 GeV, assuming that the mass difference between $\tilde{t}_1$ and $\tilde{\nu}$ is greater than 10 GeV, that $\theta_{\tilde{t}} = 0$ and that the branching fraction to each lepton flavour is the same. The 95% C.L. excluded regions in the ($m_{\tilde{t}_1}$, $m_{\tilde{\chi}^0_1}$) and ($m_{\tilde{t}_1}$, $m_{\tilde{\nu}}$) planes are shown in Figs. 8(b), 9(b) and 10(b) for various values of $\theta_{\tilde{t}}$.

5.2.2 Scalar bottom quark $\tilde{b}_1$

In order to calculate mass limits, the number of signal events passing through the event selections is determined as a function of $m_{\tilde{b}_1}$, $m_{\tilde{\chi}^0_1}$ and $\theta_{\tilde{b}}$. Fig. 11(a) shows the 95% C.L. excluded

Lower limit on $m_{\tilde{t}_1}$ (GeV)				
	$\tilde{t}_1 \to c\tilde{\chi}^0_1$		$\tilde{t}_1 \to b\ell\tilde{\nu}$ $\ell = e, \mu, \tau$	$\tilde{t}_1 \to b\tau\tilde{\nu}_\tau$ Br = 100%
$\theta_{\tilde{t}}$ (rad)	$\Delta m \geq 5$ GeV	$\Delta m \geq 10$ GeV	$\Delta m \geq 10$ GeV	$\Delta m \geq 10$ GeV
0.0	66.2	73.3	67.9	66.3
$\leq \frac{1}{8}\pi$	64.0	71.6	65.1	63.9
$\leq \frac{1}{4}\pi$	58.8	66.8	59.0	57.4
0.98	56.8	65.0	56.2	54.4

Table 7: The excluded $m_{\tilde{t}_1}$ region at 95% C.L. ($\Delta m = m_{\tilde{t}_1} - m_{\tilde{\chi}^0_1}$ or $m_{\tilde{t}_1} - m_{\tilde{\nu}}$).

regions in the ($\theta_{\tilde{b}}$, $m_{\tilde{b}_1}$) plane for the mass difference of $\Delta m (\equiv m_{\tilde{b}_1} - m_{\tilde{\chi}^0_1}) \geq 8$ GeV and $10 \leq \Delta m \leq 40$ GeV. Because the electromagnetic charge of $\tilde{b}_1$ is $-\frac{1}{3}$, the present analysis has no sensitivity to a $\tilde{b}_1$ signal if the $\tilde{b}_1$ decouples from the Z^0 boson. The numerical mass bounds are listed in Table 8 for various $\theta_{\tilde{b}}$. The lower limit on the $\tilde{b}_1$-mass is 69.7 GeV, if Δm is greater than 8 GeV and $\theta_{\tilde{b}} = 0$. The 95% C.L. excluded regions in the ($m_{\tilde{b}_1}$, $m_{\tilde{\chi}^0_1}$) plane are shown in Fig. 11(b) for various $\theta_{\tilde{b}}$.

Lower limit on $m_{\tilde{b}_1}$ (GeV) ($\tilde{b}_1 \to b\tilde{\chi}^0_1$)		
$\theta_{\tilde{b}}$ (rad)	$\Delta m \geq 8$ GeV	$10 \leq \Delta m \leq 40$ GeV
0.0	69.7	72.5
$\leq \frac{1}{8}\pi$	66.2	69.8
$\leq \frac{1}{4}\pi$	54.0	58.7

Table 8: The excluded $m_{\tilde{b}_1}$ region at 95% C.L. ($\Delta m = m_{\tilde{b}_1} - m_{\tilde{\chi}^0_1}$)

6 Summary and Conclusion

A data sample collected using the OPAL detector corresponding to an integrated luminosity of 10.4 pb^{-1} at $\sqrt{s}$ =170 and 172 GeV has been analysed to search for pair production of the scalar top quark and the scalar bottom quark predicted by the supersymmetric theories. No events remained after the selection cuts. This is consistent with the expected background of 0.44 ± 0.12 events for the $\tilde{t}_1 \to c\tilde{\chi}^0_1$ and $\tilde{b}_1 \to b\tilde{\chi}^0_1$ modes, and of 0.17 ± 0.09 events for the $\tilde{t}_1 \to b\ell\tilde{\nu}$ mode.

The 95% C.L. lower limits on the scalar top quark mass are 73.3 and 66.8 GeV, if the mixing angle of the scalar top quark is 0 and smaller than $\frac{\pi}{4}$, respectively. These limits were obtained assuming that the scalar top quark decays into a charm quark and the lightest neutralino and that the mass difference between the scalar top and the lightest neutralino is larger than 10 GeV.

Assuming a relatively light scalar neutrino (37.1 GeV $\leq m_{\tilde{\nu}} \leq m_{\tilde{t}_1} - m_b$) the complementary decay mode of the scalar top quark in which it decays into a bottom quark, a charged lepton and the scalar neutrino has also been studied. If the mass difference between the scalar top quark and the scalar neutrino is greater than 10 GeV and if the mixing angle of the scalar top

quark is 0, the 95% C.L. lower limit on the scalar top quark mass is 67.9 GeV. This limit is obtained assuming that the branching fraction to each lepton flavour is the same.

A mass limit on the light scalar bottom quark is found to be 69.7 GeV (95% C.L.), assuming that the mass difference between the scalar bottom quark and the lightest neutralino is greater than 8 GeV and that the mixing angle of the scalar bottom quark is 0.

Acknowledgements

We particularly wish to thank the SL Division for the efficient operation of the LEP accelerator at the new energies of $\sqrt{s}$ = 170–172 GeV and for their continuing close cooperation with our experimental group. We thank our colleagues from CEA, DAPNIA/SPP, CE-Saclay for their efforts over the years on the time-of-flight and trigger systems which we continue to use. In addition to the support staff at our own institutions we are pleased to acknowledge the
Department of Energy, USA,
National Science Foundation, USA,
Particle Physics and Astronomy Research Council, UK,
Natural Sciences and Engineering Research Council, Canada,
Israel Science Foundation, administered by the Israel Academy of Science and Humanities,
Minerva Gesellschaft,
Japanese Ministry of Education, Science and Culture (the Monbusho) and a grant under the Monbusho International Science Research Program,
German Israeli Bi-national Science Foundation (GIF),
Bundesministerium für Bildung, Wissenschaft, Forschung und Technologie, Germany,
National Research Council of Canada,
Hungarian Foundation for Scientific Research, OTKA T-016660, and OTKA F-015089.

References

[1] Y. Gol'fand and E. Likhtam, JETP Lett. 13 (1971) 323;
D. Volkov and V. Akulov, Phys. Lett. B46 (1973) 109;
J. Wess and B. Zumino, Nucl. Phys. B70 (1974) 39.

[2] M. Drees and K. Hikasa, Phys. Lett. B252 (1990) 127;
K. Hikasa and M. Kobayashi, Phys. Rev. D36 (1987) 724;
J. Ellis and S. Rudaz, Phys. Lett. B128 (1983) 248;
G. Altarelli and R. Rückl, Phys. Lett. B144 (1984) 126;
S. Dawson, E. Eichten and C. Quigg, Phys. Rev. D31 (1985) 1581;
J. Ellis, G.L. Fogli and E. Lisi, Nucl. Phys. B393 (1993) 3.

[3] CDF Collab., F. Abe *et al.*, Phys. Rev. D52 (1995) 2605;
D0 Collab., S. Abachi *et al.*, Phys. Rev. D52 (1995) 4877.

[4] A. Bartl, W. Majerotto, W. Porod, Z. Phys, C64 (1994) 499.

[5] D0 Collab., F. Abachi *et al.*, Phys. Rev. Lett. 76 (1996) 2222.

[6] OPAL Collab., R. Akers *et al.*, Phys. Lett. B337 (1994) 207.

[7] ALEPH Collab., D. Buskulic *et al.*, Phys. Lett. B373 (1996) 246;
DELPHI Collab., R. Keranen *et al.*, Phys. Lett. B387 (1996) 651;
L3 Collab., M. Acciarri *et al.*, Phys. Lett. B377 (1996) 289;
OPAL Collab., G. Alexander *et al.*, Z. Phys. C73 (1997) 201.

[8] OPAL Collab., K.Ackerstaff *et al.*, Phys. Lett. B389 (1996) 197.

[9] L3 Collab., O. Adriani *et al.*, Phys. Lett. B236 (1993) 1;
ALEPH Collab., D. Decamp *et al.*, Phys. Rep. 216 (1992) 253.

[10] Particle Data Group, Phys. Rev. D54 (1996) 694.

[11] OPAL Collab., K.Ackerstaff *et al.*, Phys. Lett. B389 (1996) 616.

[12] OPAL Collab., K. Ahmet *et al.*, Nucl. Instr. Meth. A305 (1991) 275;
P.P. Allport *et al.*, Nucl. Instr. Meth. A324 (1993) 34;
P.P. Allport *et al.*, Nucl. Instr. Meth. A346 (1994) 476.

[13] B.E. Anderson *et al.*, IEEE Trans. Nucl. Sci. 41 (1994) 845.

[14] T. Sjöstrand, Comp. Phys. Comm. 82 (1994) 74.

[15] B. Andersson *et al.*, Phys. Rep. 97 (1983) 31.

[16] OPAL Collab., G. Alexander *et al.*, Z. Phys. C69 (1996) 543.

[17] C. Peterson, D. Schlatter, I. Schmitt and P.M. Zerwas, Phys. Rev. D27 (1983) 105.

[18] M. Suzuki, Nucl. Phys. B258 (1985) 553.

[19] J. Allison *et al.*, Nucl. Instr. Meth. A317 (1992) 47.

[20] L. Lönnblad, M. Seymour *et al.*, in 'Physics at LEP2', eds. G. Altarelli, T. Sjöstrand and F. Zwirner, CERN 96-01, vol. 2 (1996).

[21] G. Marchesini, B.R. Webber, G. Abbiendi, I.G. Knowles, M.H. Seymour and L. Stanco, Comp. Phys. Comm. 67 (1992) 465.

[22] J.A.M. Vermaseren, Nucl. Phys. B229 (1983) 347.

[23] S. Jadach, B. F. L. Ward, Z. Wąs, Comp. Phys. Comm. 79 (1994) 503.

[24] S. Jadach, W. Płaczek, and B.F.L. Ward, in 'Physics at LEP2', eds. G. Altarelli, T. Sjöstrand and F. Zwirner, CERN 96-01, vol. 2 (1996).

[25] J. Fujimoto *et al.*, in 'Physics at LEP2', eds. G. Altarelli, T. Sjöstrand and F. Zwirner, CERN 96-01, vol. 2 (1996).

[26] S. Catani *et al.*, Phys. Lett. B269 (1991) 432.

[27] OPAL Collab., R. Akers *et al.*, Phys. Lett. B327 (1994) 411;
OPAL Collab., R. Akers *et al.*, Z. Phys. C65 (1994) 17.

[28] OPAL Collab., P. Acton *et al.*, Z. Phys. C58 (1993) 523;
OPAL Collab., R. Akers *et al.*, Z. Phys. C60 (1993) 199.

[29] LEP Energy Calibration in 1996, The working group on LEP energy, March 1997.

[30] M.G. Bowler, Z. Phys. C11 (1981) 169.

[31] OPAL Collab., K. Ackerstaff *et al.*, Phys. Lett. B391(1997) 221-234.

[32] F.A. Berends, R. Pittau, R. Kleiss, Comp. Phys. Comm. 85 (1995) 437.

[33] R.D. Cousins and V.L. Highland, Nucl. Instr. Meth. A320 (1992) 331.

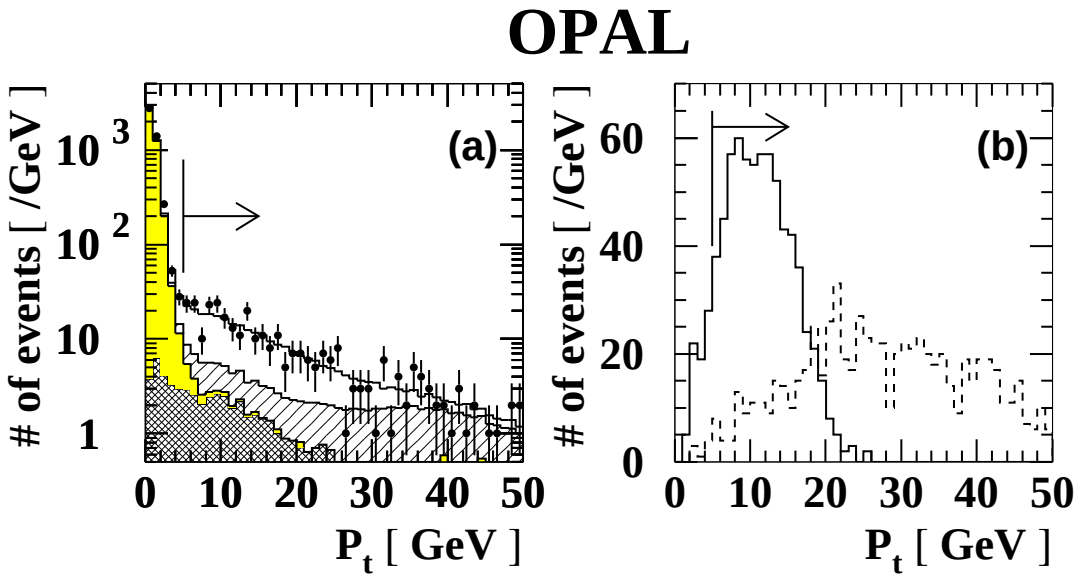

Figure 1: The distributions of P_t after cut (P3) for background (histograms) and data in (a), and for $\tilde{t}_1\bar{\tilde{t}}_1$ predictions in (b). The arrows in these figures show the selection criteria. In (a) the distribution of the data is shown by the points with error bars. The predictions from background processes are also shown: dilepton events (cross hatched area), two-photon processes (grey area), four-fermion processes (singly hatched area), and multihadronic events (open area). (b) shows predictions for $\tilde{t}_1\bar{\tilde{t}}_1$ in which $\tilde{t}_1$ decays into $c\tilde{\chi}_1^0$. The continuous line histogram is for $(m_{\tilde{t}_1}, m_{\tilde{\chi}_1^0})$ =(70 GeV, 60 GeV), and the dashed line is for (70 GeV, 35 GeV), starting from 1000 generated events for each.

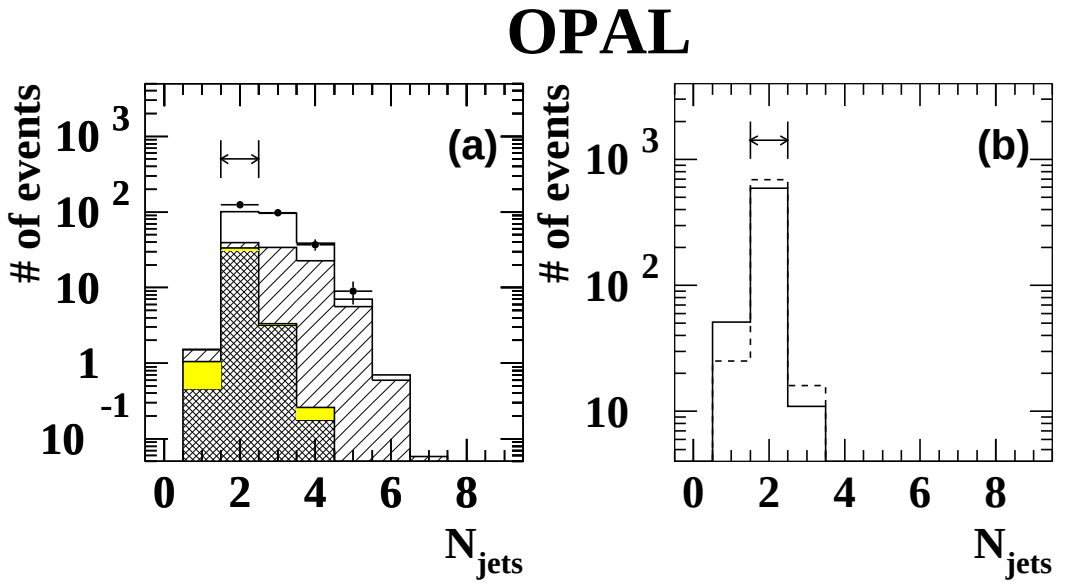

Figure 2: The distributions of the number of reconstructed jets after all preselections: for background (histograms) and data in (a), and for $\tilde{t}_1\bar{\tilde{t}}_1$ predictions in (b). The conventions for the various histograms are the same as in Fig. 1.

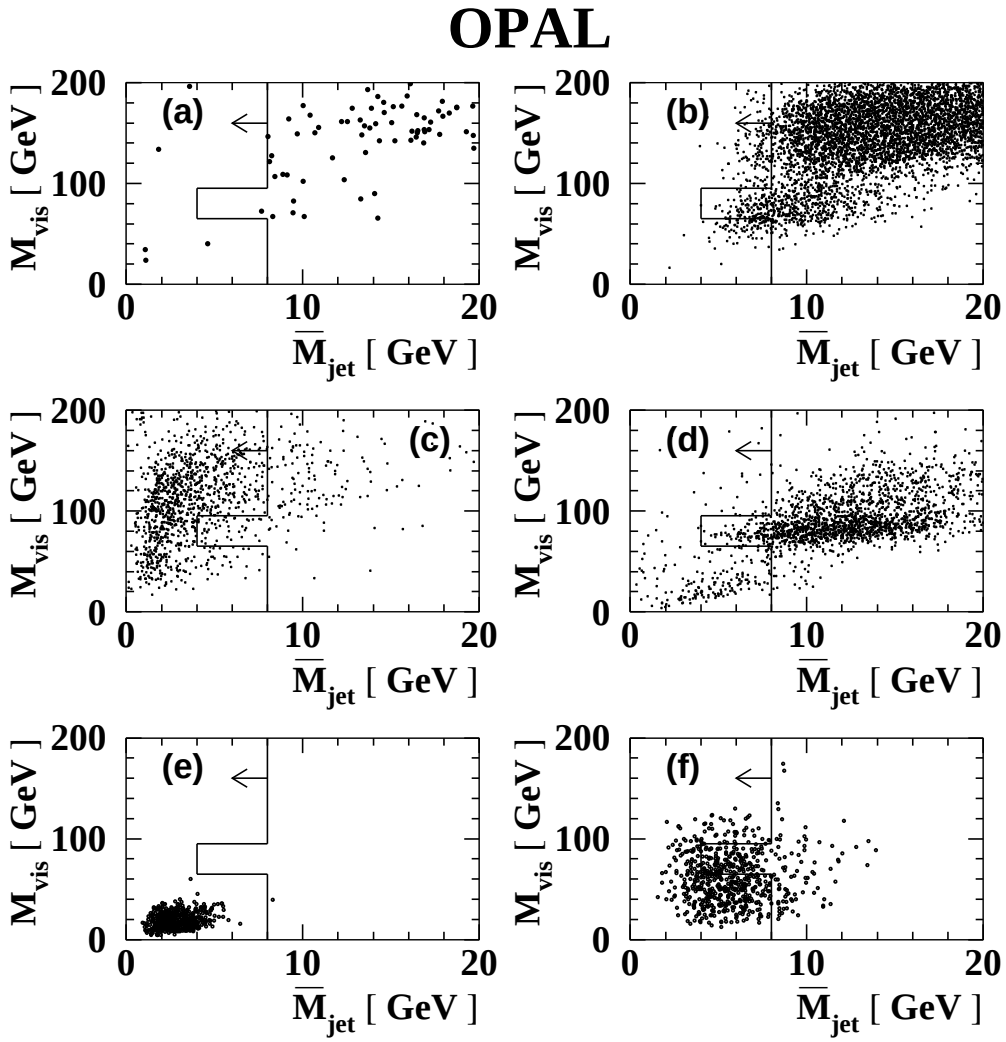

Figure 3: Scatter plots of $M_{\rm vis}$-$\bar{M}_{\rm jet}$ for (a) data, (b) simulated multihadronic events, (c) simulated $\ell\ell$ events, (d) simulated four-fermion processes ($\mathrm{W^+W^-}$, Weν, $\gamma^*\mathrm{Z^0}$ and $\mathrm{Z^0ee}$) and (e),(f) the Monte Carlo simulation of $\tilde{\mathrm{t}}_1\bar{\tilde{\mathrm{t}}}_1$ signals of ($m_{\tilde{\mathrm{t}}_1}$,$m_{\tilde{\chi}^0_1}$)=(70 GeV, 60 GeV), (70 GeV, 0 GeV). The simulated events are not normalised to the luminosity.

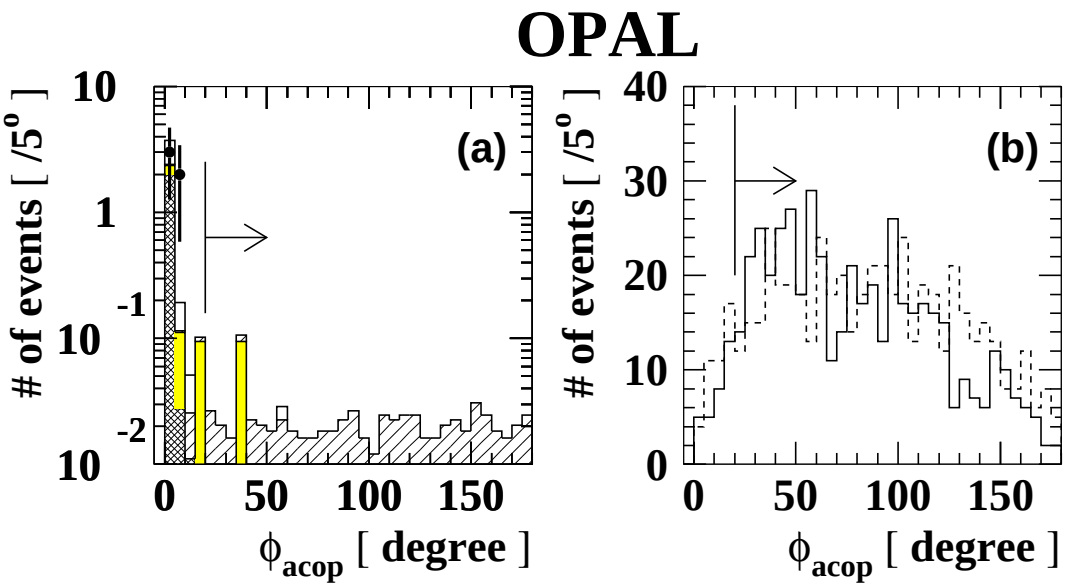

Figure 4: The distributions of the acoplanarity angle after cut (A3) for background (histograms) and data in (a), and for the $\tilde{t}_1\bar{\tilde{t}}_1$ predictions in (b). The conventions for the various histograms are the same as in Fig. 1.

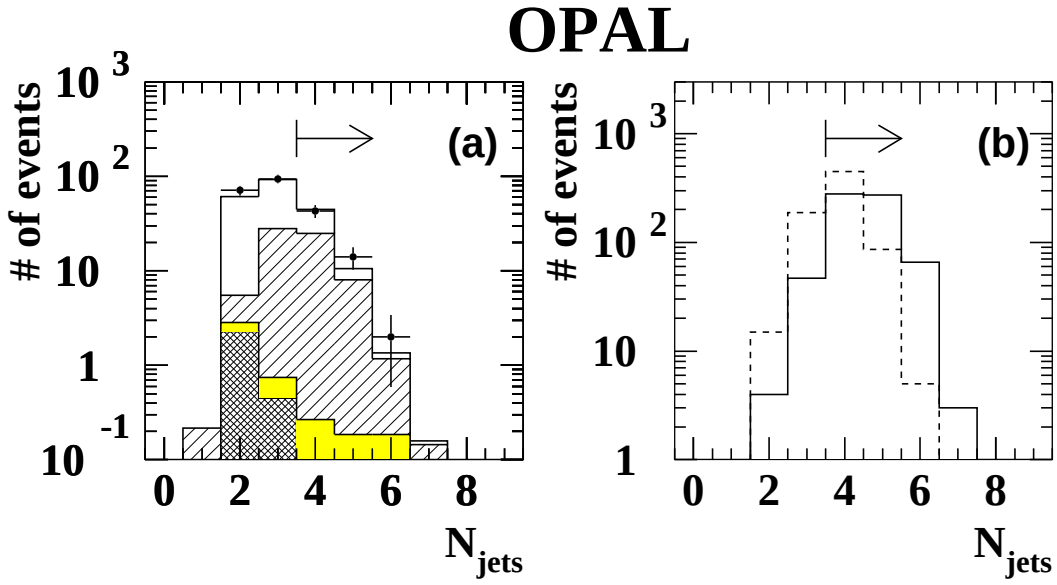

Figure 5: The distributions of the number of reconstructed jets after cut (B1). The arrows in these figures show the selection criteria. (a) shows the distribution of the data with error bars. The predictions from background processes are also shown: dilepton events (cross hatched area), two-photon processes (grey area), four-fermion processes (singly hatched area), and the multihadronic events (open area). (b) shows predictions for $\tilde{t}_1\bar{\tilde{t}}_1$ in which $\tilde{t}_1$ decays into $b\ell\tilde{\nu}$. The continuous line histogram is for $(m_{\tilde{t}_1}, m_{\tilde{\nu}})$ =(70 GeV, 55 GeV), and the dotted line is for (70 GeV, 35 GeV). In these samples, the branching fraction to each lepton flavour is assumed to be the same.

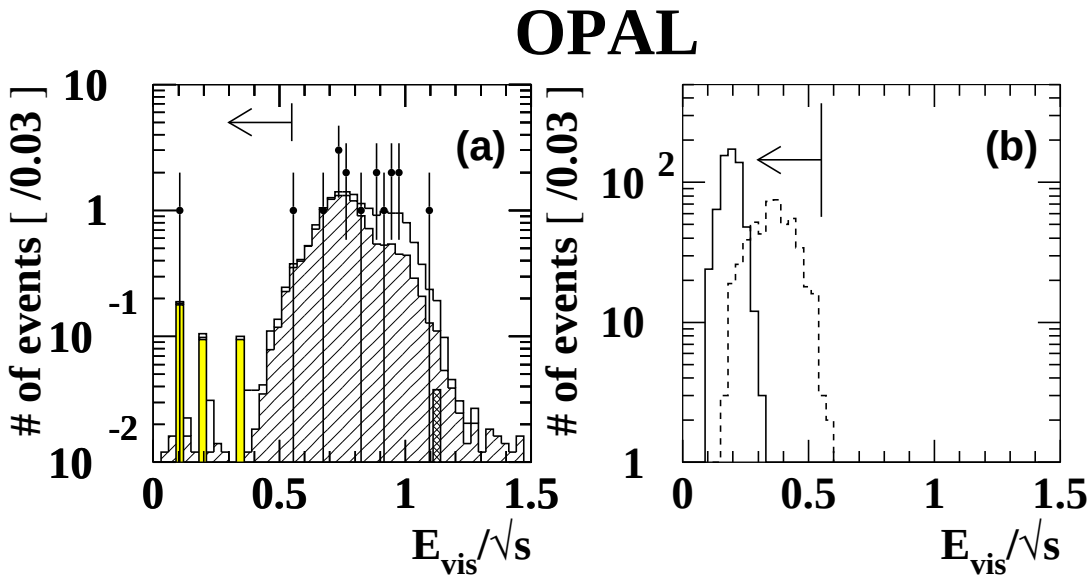

Figure 6: The distributions of the visible energy normalised to the centre-of-mass energy after cut (B3) for background (histograms) and data in (a), and for the $\tilde{t}_1\bar{\tilde{t}}_1$ signal predictions in (b). The conventions for the various histograms are the same as in Fig. 5.

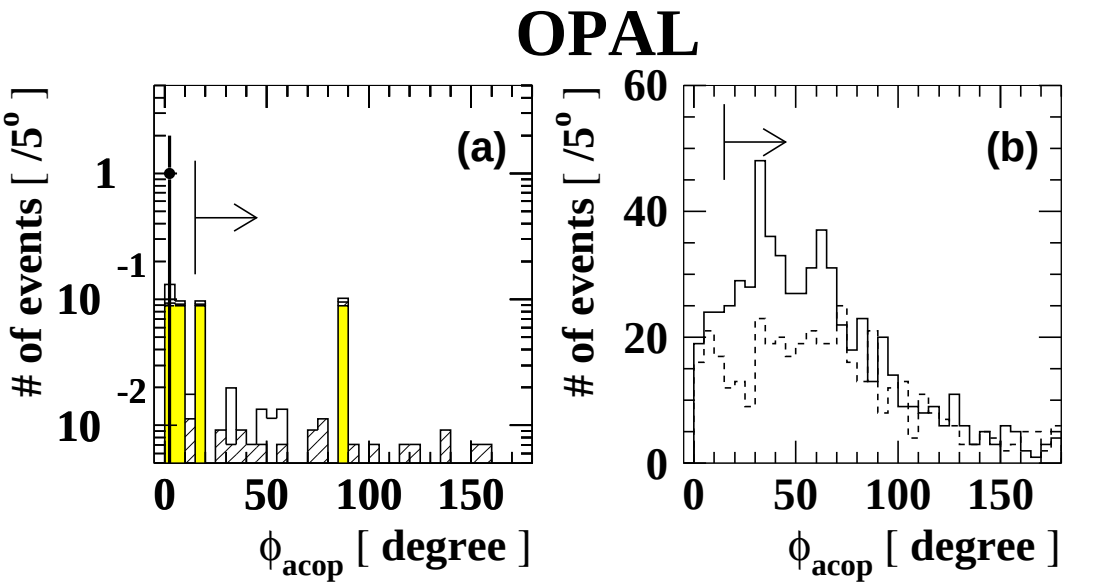

Figure 7: The distributions of the acoplanarity angle after cut (B5) for background (histograms) and data in (a), and for the $\tilde{t}_1\bar{\tilde{t}}_1$ predictions in (b). The conventions for the various histograms are the same as in Fig. 5.

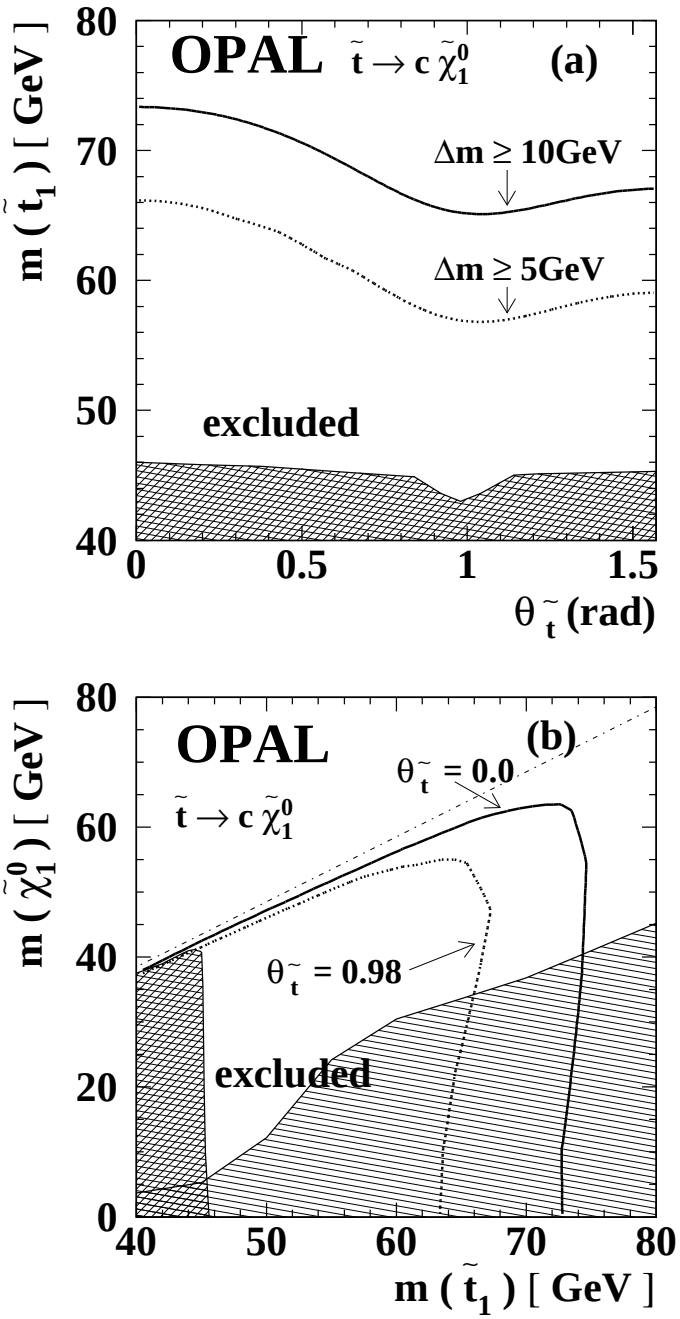

Figure 8: The 95% C.L. excluded regions assuming that the $\tilde{t}_1$ decays into $c\tilde{\chi}_1^0$.
(a) The excluded regions in the $(\theta_{\tilde{t}}, m_{\tilde{t}_1})$ plane. The solid line shows the limit for a mass difference $\Delta m\,(= m_{\tilde{t}_1} - m_{\tilde{\chi}_1^0}) \geq 10$ GeV, and the dotted line for $\Delta m \geq 5$ GeV. The cross hatched region has already been excluded by the search at LEP1 [6].
(b) The excluded regions in the $(m_{\tilde{t}_1}, m_{\tilde{\chi}_1^0})$ plane, for a mixing angle of $\tilde{t}_1$ of 0.0 (solid line) and 0.98 rad (dotted line). The cross hatched region has already been excluded by the search at LEP1 [6]. The singly hatched region has been excluded by the D0 Collaboration [5]. The dash-dotted straight line shows the kinematic limit for the $\tilde{t}_1 \to c\tilde{\chi}_1^0$ decay.

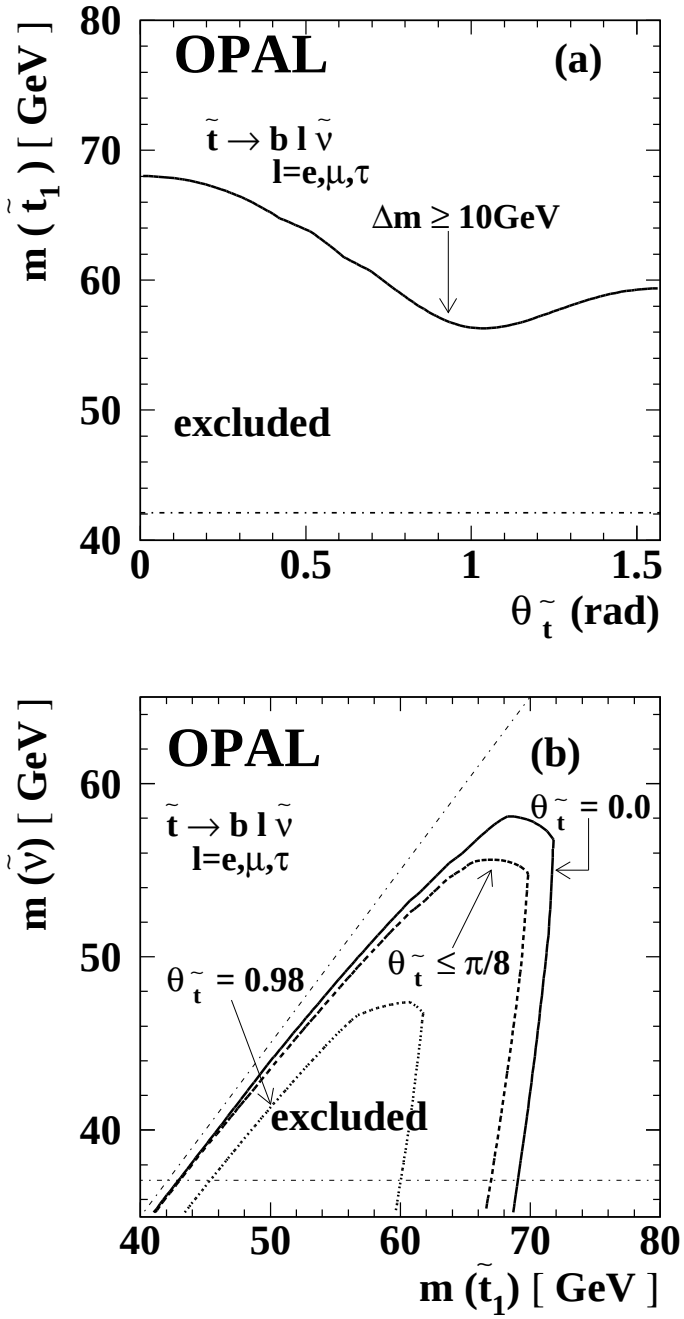

Figure 9: The 95% C.L. excluded regions assuming that the $\tilde{t}_1$ decays into b$\ell\tilde{\nu}$ and that the branching fraction to each lepton flavour is the same.
(a) The excluded regions in the ($\theta_{\tilde{t}}$, $m_{\tilde{t}_1}$) plane where the mass difference between the $\tilde{t}_1$ and the $\tilde{\nu}$ is greater than 10 GeV. The dash-dotted straight line shows the kinematic limit for this decay, since a $\tilde{\nu}$ lighter than 37.1 GeV has been excluded [9, 10].
(b) The excluded regions in the ($m_{\tilde{t}_1}$, $m_{\tilde{\nu}}$) plane, for a mixing angle of the $\tilde{t}_1$ assumed to be 0.0 (solid line), smaller than $\pi/8$ rad (dashed line), and 0.98 rad (dotted line). The dash-dotted horizontal line shows the limit on $m_{\tilde{\nu}}$ obtained at LEP1, and the dash-dotted diagonal line shows the kinematic limit for the $\tilde{t}_1 \to b\ell\tilde{\nu}$ decay.

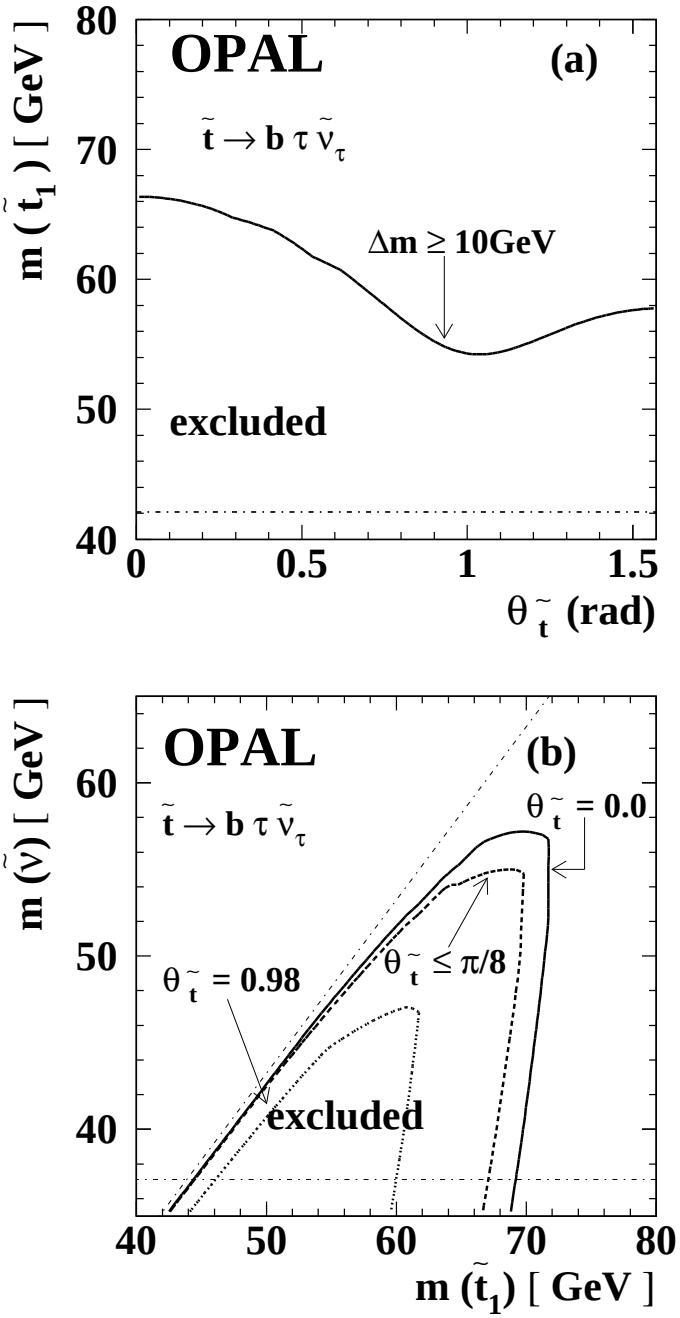

Figure 10: The 95% C.L. excluded regions assuming that $\tilde{t}_1$ always decays into $b\tau\tilde{\nu}_\tau$.
(a) The excluded regions in the $(\theta_{\tilde{t}}, m_{\tilde{t}_1})$ plane where the mass difference between the $\tilde{t}_1$ and the $\tilde{\nu}_\tau$ is greater than 10 GeV. The dash-dotted straight line shows the kinematic limit for this decay, since a $\tilde{\nu}$ lighter than 37.1 GeV has been excluded [9, 10].
(b) The excluded regions in the $(m_{\tilde{t}_1}, m_{\tilde{\nu}})$ plane, for a mixing angle of the $\tilde{t}_1$ assumed to be 0.0 (solid line), smaller than $\pi/8$ rad (dashed line), and 0.98 rad (dotted line). The dash-dotted horizontal line shows the limit on $m_{\tilde{\nu}}$ obtained at LEP1, and the dash-dotted diagonal line shows the kinematic limit for the $\tilde{t}_1 \to b\tau\tilde{\nu}$ decay.

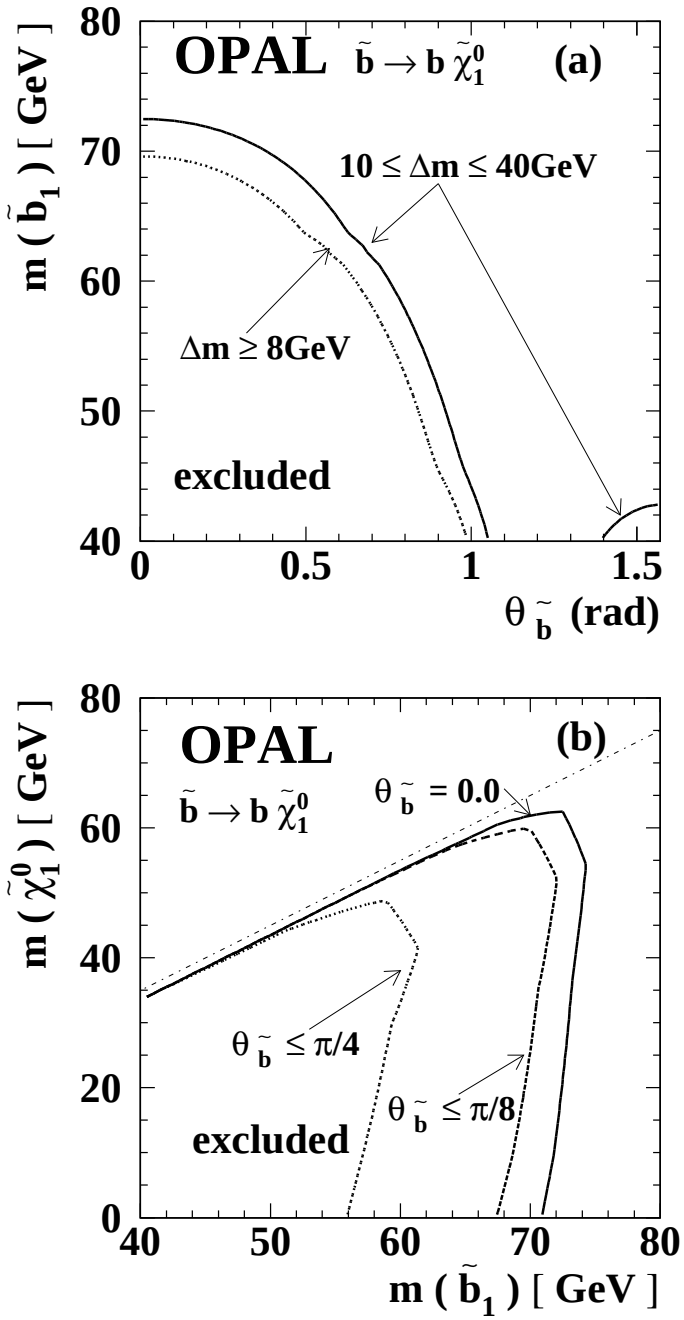

Figure 11: The 95% C.L. excluded regions assuming that the $\tilde{b}_1$ decays into $b\tilde{\chi}_1^0$.
(a) The excluded region in the $(\theta_{\tilde{b}}, m_{\tilde{b}_1})$ plane for a mass difference, $\Delta m\,(= m_{\tilde{b}_1} - m_{\tilde{\chi}_1^0})$, $10 \le \Delta m \le 40$ GeV. The dotted line shows the excluded region for $\Delta m \ge 8$ GeV.
(b) The excluded regions in the $(m_{\tilde{b}_1}, m_{\tilde{\chi}_1^0})$ plane, for a mixing angle of the $\tilde{b}_1$ assumed to be 0.0 (solid line), smaller than $\pi/8$ rad (dashed line), and smaller than $\pi/4$ (dotted line). The dash-dotted line shows the kinematic limit for the $\tilde{b}_1 \to b\tilde{\chi}_1^0$ decay.